On the Source of Midlatitude Low-Frequency Variability. Part II: Nonlinear Equilibration of Weather Regimes

ROBERT VAUTARD* AND BERNARD LEGRAS

Laboratoire de Météorologie Dynamique, 75231 Paris Cedex 05, France

(Manuscript received 27 July 1987, in final form 8 April 1988)

ABSTRACT

We present a new statistical–dynamical approach to the concept of weather regimes, including the effect of transients, without any assumption other than scale separation. The method is applied to a quasi-geostrophic channel model without topography and forced by a local baroclinic jet. Baroclinic perturbations grow and decay along a storm track which is linked with a maximum of low-frequency variability towards its exit, in agreement with the observations.

The weather regimes are searched within the subspace spanned by the large scales only. They are identified through the resolution of a stationary problem in which the feedback of the transients is included as an ensemble average over analogs of the large-scale flow. In this way, the feedback is a continuous function of the large-scale flow only, and the system of equations is closed, taking into account the whole coupling. The solution is obtained using a nonlinear optimization technique.

Several regimes are identified corresponding to zonal and blocking situations. The blocking flow is characterized by a well-marked barotropic dipole at the end of the storm track of synoptic perturbations. The feedback term is shown to act positively in both cases though there are major differences between zonal and blocking regimes. In particular we show that the dipole of the blocking flow is essentially maintained against dissipation by the small-scale fluxes. It is shown that full nonlinearity is required to explain the observed behavior.

The efficiency of the method in this simple case allows us to discuss its extension to a more ambitious diagnostic of regimes in atmospheric observations as well as GCM simulations.

1. Introduction

In Part I of this paper (Vautard et al. 1988; hereafter referred to as Part I), we investigate the dynamics of a quasi-geostrophic flow forced by a localized baroclinic jet. Although based on a rather simple design, the model exhibits realistic behavior, and reproduces the main features of the observed dynamics of synoptic and large-scale waves. The persistence properties of the large-scale flow are shown to be inhomogeneously distributed in phase space. Maximal probability of persistence occurs for two different flows which resemble respectively observed zonal and blocking circulations. Compositing the potential vorticity fluxes over the blocking cases shows that transients clearly tend to reinforce the block.

The previous study is based on pure diagnostic analysis of the model data. It does not incorporate explicitly any dynamical information about the balance of the analyzed fields, and thus cannot reach an accurate definition of quasi-stationary weather regimes. In addition, several subjective parameters are involved in pattern analysis which cannot be completely justified on a rigorous basis. The aim of Part II is to provide an objective definition of weather regimes, using dynamical information, and to show that it can be operationally used and yield results in agreement with Part I.

The main difficulty is that within a persistent sequence the quasi-stationary large-scale flow is coupled with small-scale disturbances. On one hand, the synoptic activity depends on the large-scale flow and on the other, the feedback of the transients onto the large-scale flow is a factor of the maintenance of this latter. The mechanism of this feedback loop has to be taken into account and parameterized if one wishes to close the formulation of the problem in terms of quasi-stationary modes only. It would not make sense here to freeze the small scales and try to find the stationary solutions of the original equations of motion as it can be done within a pure barotropic framework (Legras and Ghil 1985). Alternately, one may try to represent the effect of the transients by the feedback of the most unstable linear mode of the current large-scale flow. Reinhold and Pierrehumbert (1982) found in this way the quasi-stationary equilibria of a simple baroclinic model with orography. However, in a more realistic

* Present affiliation: Department of Atmospheric Sciences, University of California, Los Angeles, California.

Corresponding author address: Dr. Bernard Legras, Laboratoire de Meteorologie Dynamique, Ecole Normale Supérieure, 24 rue Lhomond, 75231 Paris Cedex 05, France.

formulation including many degrees of freedom, this method is questionable as soon as we are not close to marginal stability and as several instabilities compete at finite amplitude. In addition, Itoh (1985) showed that the average energetics of chaotic baroclinic dynamics differ significantly from the energetics of stationary states and their most unstable modes.

In this article, we develop a new approach for the determination of quasi-stationary regimes. The feedback from small-scale transients is parameterized in a diagnostic way using a long-term integration of our model. The feedback is calculated as a continuous function of the large-scale flow and is used to close the statistical–dynamical equations of the quasi-stationary flow. An optimization procedure then yields the solutions of these equations. The resulting flow achieves a nonlinear equilibration between dissipation, advection and transient feedback.

In section 2, we briefly review the main characteristics of the model and the results of Part I, and specify our definition of weather regimes. In section 3, the equilibration method applied for the recognition of weather regimes is presented. The application to our model is reported in section 4 with an accompanying discussion on the statistical significance and the stability of the obtained solutions. In this section, we also justify our approach by measuring the role of transients in the equilibration balance. In section 5, we compare our results with the persistence properties measured in Part I. Section 6 shows the inadequacy of a linear parameterization of the transients. Section 7 contains a summary and further discussion.

2. A quantitative approach to weather regimes

a. The model

In Part I, we investigate the behavior of a quasi-geostrophic two-level model with a periodic channel geometry. The basic state ψ^* (Fig. 1 of Part I) consists of a mean zonal wind with an unstable vertical shear superimposed on a local jet within the first quarter of the upper level. An appropriate forcing maintains ψ^* as a stationary solution. The baroclinic eddies are generated within the strong baroclinic jet and advected downstream along a storm track. They tend to reduce the baroclinity of the mean flow and to extend the jet further downstream. The storm track is shown to connect the jet with a region of low-frequency variability located near its downstream exit. The distribution of large-scale variance shows a preference for some flow patterns which can be classified into zonal and blocked types of circulation. A detailed study of the persistence properties (which will be further elaborated on in section 5) shows that these patterns are associated with extrema of the probability of persistence.

The potential vorticity equations (Eq. 2.2 of Part I) are integrated with the same set of parameter values as in Part I. We restate the main ones here:

upper radius of deformation	$R_1 = 500$ km
lower radius of deformation	$R_2 = 707$ km
upper mean wind	$U_1 = 18$ m s^{-1}
lower mean wind	$U_2 = 6$ m s^{-1}
maximum local shear	$m = 37$ m s^{-1}
internal friction	23.1 days
Ekman decay	3.9 days

These values are such that the external barotropic mode (3, 2) would be stationary in absence of the enhanced jet. However, as seen in Part I, a relatively large variation of $U = \frac{1}{2}(U_1 + U_2)$ only slightly affects the behavior of the model, showing that sharp resonance is not a key factor here. For a further discussion about these parameters and the sensitivity of the circulation to their values, the reader is referred to Part I. All notations are identical in the two papers.

b. Definition of weather regimes

The notion of weather regimes originates from the empirical observation that quasi-stationary persistent large-scale anomalies repeatedly occur at some locations (Rex 1950). The long duration of blocking events, often exceeding the spin-down time scale, inclines one to think that a specific dynamical balance of the large-scale flow is required. Advection and dissipation must be equilibrated by a forcing either due to large-scale instabilities or to transient feedback. The former possibility embodies both the orographic form drag (Charney and DeVore 1979) and any kind of large-scale baroclinic instabilities triggered by the orography or heat sources. When considered alone, this family of factors leads to weather regimes as multiple stationary solutions for the large-scale flow. Various barotropic and baroclinic models have been studied for this purpose in a number of recent studies.

When both large-scale instabilities and transient feedback are taken into account, the problem is far more complex unless one is able to calculate the statistical effects of the transients as a function of the stationary part of the field. If, as we show later, this difficulty is solved, the problem reduces to finding stationary solutions of a dynamical–statistical equation for the large-scale flow. The first step to the solution is to observe that a given large-scale flow may undergo different instantaneous deformations depending on the superimposed small-scale eddies. We then define the *statistical tendency* as the average of the instantaneous tendency (time derivative) over all physically realizable situations having the same large-scale component. Two observable realizations of a large-scale pattern only differ by the associated simultaneous small-scale flow. Regardless of the evolution process for the latter, we consider the small scales as well as the instantaneous tendencies as random variables whose probability density distribution depends on the large-scale configuration. Under the Gaussian approximation, it is well known that the statistical tendency, so defined, is the

best constant estimate of the instantaneous tendency. Accordingly, we define the large-scale *regimes* as the large-scale patterns whose statistical tendency vanishes. Note that Dole and Gordon (1983) have used a similar formulation for the variation of the geopotential anomaly at one single geographical location.

The application of the above definition is made easier by the observation that quasi-stationary and traveling waves in the atmosphere (Fraedrich and Böttger 1978; Hayashi 1982) and in our model (cf. section 4 of Part I) separate rather well in the frequency–wavenumber domain. In other words, there is, to a first approximation, an appropriate cut in wavenumber domain which separates two ranges of low and high temporal frequency variability with limited overlap. In this study, the large scales include the Fourier modes of the channel with zonal wavenumber $k \leqslant 3$ and meridional wavenumber $l \leqslant 2$ and the small scales embody the remaining modes.

Accordingly, we can now formulate the problem in a more quantitative way. The vorticity field $q = (q_1, q_2)$ for the two levels is split into a large-scale part L and a small-scale part S:

$$q = L + S, \tag{2.1}$$

where L and S are two amplitude vectors in the subspaces of large- and small-scale modes, respectively.

Since the quasi-geostrophic approximation only involves quadratic nonlinearities, the evolution equation for the component L reads

$$\frac{\partial L}{\partial t} = A(L) + B(L, S) + C(S, S). \tag{2.2}$$

The right-hand side is separated into three contributions. The function A groups all linear and constant terms, and the nonlinear self-interactions of large scales. In a classical low-order truncation, the model would be closed by retaining only this contribution. The B and C terms are bilinear and group the mixed L–S interactions (B) and the S–S interactions (C). Actually, nonlinear interactions are organized as triads in phase space and the B and C terms are the projections of the contributions of (L, L, S) and (L, S, S) triads onto the large scales. As stated above, the average is taken over observable transients for the current configuration of the large-scale flow. Denoting this average (which we will discuss later) as an overbar, the statistical tendency for L reads

$$T(L) = \overline{A(L)} + \overline{B(L, S)} + \overline{C(S, S)}, \tag{2.3}$$

where $\overline{A(L)} = A(L)$, $\overline{C(S, S)} = \tilde{C}(L)$ and $\overline{B(L, S)} = B(L, \bar{S}) = B(L, \tilde{S}(L)) = \tilde{B}(L)$. Here all the terms depend only on the large-scale part of the flow, thus closing Eq. (2.2). The term $\tilde{C}$ is a Reynolds stress and $\tilde{B}$ does not vanish since we allow the average $\bar{S} = \tilde{S}(L)$ to differ from zero (yet it has to be small). In section 4, we discuss in detail all these terms.

Our approach is to approximate the average operator in a diagnostic way using the data generated by a long-term integration of the complete model. The statistical tendency associated with a given large-scale flow is estimated by compositing over encountered situations which exhibit close enough large-scale flows. We show below how the small-scale fluxes can be computed as continuous functions of the large-scale modal amplitudes.

This formulation can be understood using dynamical systems theory: the phase space is the sum of the orthogonal subspaces spanned by the small scales and the large scales. The dynamical system given by the full prognostic equations possesses an asymptotic climatic attractor for each point of which the instantaneous large-scale tendency is the projection of the "speed vector" onto the large-scale subspace. The statistical tendency of a point in this subspace is then given by the average of these projections taken over all crossings with the subspace parallel to the small-scale subspace containing that point, as sketched in Fig. 1. The possible discontinuities arising from this definition can be smoothed out by a further average in a small neighborhood of the considered point. Note that there are, generally, infinitely many trajectories which project on an arbitrary small neighborhood of L but the selection is far different from choosing S at random because the attractor itself occupies an extremely small fraction (of measure zero) of the a priori accessible phase space.

Thus we call weather regimes the solutions of

$$T(L) = 0, \tag{2.4}$$

for which a statistical equilibration occurs between self-interaction and feedback from the small scales, as defined above. The mere significance of the equilibration problem (2.4) relies on the fact that large scales gen-

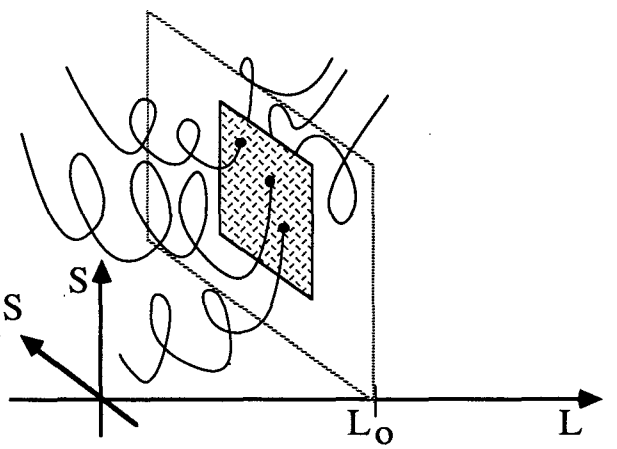

FIG. 1. In this phase-space representation, the large-scale modes (L) are figured by the horizontal axis and the small-scale modes (S) by the two other axes. The statistical tendency for L_0 is obtained by averaging over all the instantaneous tendencies of the solution trajectories as they intersect the plane $L = L_0$.

erally vary over longer time scales than the small scales, except for some unfrequent abrupt transitions.

Before we tackle the resolution of Eq. (2.4) in the next subsection, we need to state precisely how $\tilde{S}$ and $\tilde{C}$ are, in practice, determined as a function of L. We have already mentioned that the method consists of using the archives of a long integration of the full model to find the periods during which the large-scale flow is an analog to the current configuration L, and to compute the averaged transient terms for L over the selected periods. More precisely, we archive N periods of duration τ; for each, we compute a time-average large-scale flow

$$L_i = \frac{1}{\tau}\int_{(i-1)\tau}^{i\tau} L(t)dt,$$

and similarly an average small-scale pattern S_i and an average Reynolds stress C_i, with $i = 1, \cdots, N$. Then for a given L, we define

$$\tilde{S}(L) = \sum_{i=1}^{N} w(L, L_i)\cdot S_i, \tag{2.5}$$

$$\tilde{C}(L) = \sum_{i=1}^{N} w(L, L_i)\cdot C_i, \tag{2.6}$$

where w is a weight factor, actually a function of a distance $d(L, L_i)$ between L and L_i in phase space and differing from zero only when d is sufficiently small. For reasons that will be detailed shortly, w must be continuous and differentiable in L.

In order to have a sufficient sampling of our attractor we perform a long integration of 15 000 days of our model. We actually use the first of the three 15 000-day integrations described in Part I, and the second one is used to estimate the significance of the solutions. Vautard (1987) shows that the decay time of the spatial correlation is about 10 days for the large scales and 5 days when all scales are retained. Thus, we choose to take $\tau = 5$ days, so that $N = 3000$ periods are retained from our integration. For each individual period, the averages of the large scales L_i, the small scales S_i and the Reynolds stress C_i are computed using a primary twice-daily archive.

The subspace wherein large-scale solutions are explored is somewhat restricted by keeping the antisymmetric part of the streamfunction field only in L. This simplification proceeds from the observation that these modes largely dominate the coherent low-frequency variability (see section 4 of Part I); it is formally equivalent to solve Eq. (2.4) for antisymmetric solutions only. Then the number of degrees of freedom reduces to 14 with one zonal mode (0, 2) and six wavy real modes (1, 2), (2, 2) and (3, 2) at each level. For the consistency of the stationary hypothesis, the feedback of symmetric large-scale transients onto the antisymmetric large-scale flow is not taken into account. With this choice, A reduces to a linear term in ψ_L, and the sole solution of $A(L) = 0$ is close to $\psi\mathfrak{T}$. Still, it is rather clear that $\psi\mathfrak{T}$ is not a solution of Eq. (2.4) as soon as transients induce a nonzero feedback onto the large-scale flow. Neither is the average large-scale flow over the whole experiment a solution of Eq. (2.4). Though the tendency averaged over the 15 000 days almost vanishes, as it is natural for a bounded flow, the statistical tendency computed over the neighborhood of the mean flow may not vanish. In other words, the barycenter of an attractor is not necessarily a remarkable point by itself and in most cases is not in local balance.

The following points are noted:

1) When the large-scale dynamics is characterized by quasi-stationary periods interrupted by abrupt transitions, we can deduce that the quasi-stationary patterns are solutions of the equilibration problem since the branches of the attractor that project onto their neighborhoods are parallel to the small-scale subspace.

2) A difficulty in our definition of weather regimes is that some nonpersistent patterns could be obtained as solutions of Eq. (2.4). Indeed, several branches of the attractor, oriented toward different directions, may contribute by projection to a vanishing average tendency. It is thus necessary to check for the persistence of the solutions of Eq. (2.4). This is done in section 5 of this study. Note, in addition, that the effects of superimposed projections may more generally induce a shift of the apparent solution from a persistent circulation.

3) The spurious solutions due to the previous effect are unlikely as the dimension of the phase-space increases.

4) We exclude from our analysis nonpersistent regularities of the large-scale flow such as long-wave propagation, which may occur as frequently as quasi-stationary events. In the final discussion we give insights on how to extend our approach to this more general case.

5) A closely related definition of weather regimes is used by Reinhold and Pierrehumbert (1982). These authors first compute the most unstable eigenmode of the current large-scale flow and then parameterize the small-scale effects as the phase-average feedback of this mode artificially assigned to a fixed amplitude. This quasi-linear method bears the advantage of being prognostic but contains more arbitrary settings than ours. Furthermore, we show in section 6 that, at least in our model, the transient feedback is not adequately described by the behavior of the most unstable mode.

3. Equilibration method

Our aim here is to show how we can solve the nonlinear system of Eq. (2.4) with a minimum amount of computations. This section presents some original developments but can be skipped by the reader who is only interested in the obtained solutions. Since the

number of modes retained in L is small, the problem can be treated using Newton's method. (Legras and Ghil 1985). However, the $\tilde{C}(L)$ and $\tilde{S}(L)$ terms in the tendency equation have to be differentiated with respect to all components of L at each step of the method, using Eqs. (2.5) and (2.6). It is thus interesting to first transform the problem into the minimization of a scalar function for which a single gradient vector is involved.

This is easily done by defining a cost function

$$F(L) = \frac{1}{2}\langle T(L), T(L)\rangle, \tag{3.1}$$

where $\langle \cdot, \cdot \rangle$ is the inner product associated with the energy. More precisely, if $q = (q_1, q_2)$ and $q' = (q'_1, q'_2)$ are two potential vorticity fields, and (ψ_1, ψ_2), (ψ'_1, ψ'_2) the associated streamfunctions, we read

$$\langle q, q'\rangle = \int\int [R_1{}^2\nabla\psi_1\cdot\nabla\psi'_1 + R_2{}^2\nabla\psi_2\cdot\nabla\psi'_2 + (\psi_1 - \psi_2)(\psi'_1 - \psi'_2)]dxdy, \tag{3.2}$$

where the integral is computed over the channel.

Starting from a given distribution of large-scale components $L^{(0)}$, and using the quasi-Newtonian method detailed in appendix A, we minimize F by successive iterations of the algorithm. This calculation may yield local minima, where F does not vanish. Solutions of Eq. (2.4) are reached when the successive values of F converge to zero.

At each step the method requires the knowledge of the gradient $\nabla_L F(L)$ of F with respect to L, defined by

$$dF = \langle \nabla_L F(L), dL\rangle \tag{3.3}$$

for the departure dF from $F(L)$ induced by an arbitrary variation dL from L. Equation (3.3) shows that the gradient depends on the chosen inner product in (3.1). In an orthonormal basis for the inner product, the gradient reduces to the set of the partial derivatives of F with respect to the components of L. With the definition (3.1) one obtains

$$dF = \left\langle T(L), \frac{DT}{DL}(L)\cdot dL\right\rangle, \tag{3.4}$$

where DT/DL is the differential operator of T. Using properties of *adjoint operators* (Talagrand and Courtier 1987), we immediately obtain an expression for the gradient

$$\nabla_L F(L) = \left(\frac{DT}{DL}(L)\right)^*\cdot T(L), \tag{3.5}$$

where the asterisk denotes the adjunction for the inner product $\langle \cdot, \cdot \rangle$.

It can be seen in the following examples that this algebraic apparatus leads to a real simplification of the computations. First, let $T(\psi)$ be the truncated form of the Jacobian $J(\psi, \Delta\psi)$ where ψ and T are truncated expansions of the streamfunction and the tendency in wavenumber space. Let us also denote by M the prescribed symmetric matrix or operator of the inner product $\langle \cdot, \cdot \rangle$, such that

$$F = \frac{1}{2}\langle T, T\rangle = \frac{1}{2}T^T\cdot M\cdot T = \frac{1}{2}\int\int TMTdxdy.$$

Using the orthogonal basis of eigenfunctions of the Laplacian, we can formally use the matrix product or the continuous integral formulation at our convenience. Then dF becomes

$$dF = \int\int T(\psi)M[J(\psi, \Delta d\psi) + J(d\psi, \Delta\psi)]dxdy.$$

Through integration by parts,

$$dF = -\int\int d\psi[\Delta J(\psi, MT(\psi)) + J(MT(\psi), \Delta\psi)]dxdy.$$

The gradient is in this case

$$\nabla_\psi F(\psi) = -M^{-1}[\Delta J(\psi, MT(\psi)) + J(MT(\psi), \Delta\psi)]dxdy. \tag{3.6}$$

A second example arises when $T(L)$ is truncated to the $\tilde{C}$ term in (2.3). The dependence in L is then entirely contained within the weight factors, and we obtain

$$dF = T^T(L)\cdot M\cdot \sum_{i=1}^{N}\left(\frac{Dw}{DL}(L, L_i)\cdot dL\right)C_i,$$

where Dw/DL is the vector of partial derivatives of w with respect to the components of L. The adjoint is now

$$\nabla_L F(L) = M^{-1}\sum_{i=1}^{N}\langle T(L), C_i\rangle\left(\frac{Dw}{DL}(L, L_i)\right). \tag{3.7}$$

In both examples, the computation of the gradient requires a number of operations proportional to the number N_L of modes in L, as in the evaluation of T itself. In Newton's method, the number of operations would grow much more rapidly as $N_L{}^2$ and, practically, the quasi-Newton's method is interesting even for small values of N_L. With $T(L)$ defined as in Eq. (2.3), the calculation of the adjoint operator $(DT/DL)^*$ combines the two above examples. Complete formulas are given in appendix B.

Equation (3.7) for the adjoint requires that the weight function w is differentiable in order to ensure the smoothness of F. We define

$$w(L, L_i) = \frac{\phi(d(L, L_i))}{\sum_{j=1}^{3000}\phi(d(L, L_j))}. \tag{3.8}$$

In (3.8), $d(L, L_i)$ is the Euclidian distance between L and L_i, and ϕ is the proximity function defined as

$$\phi(x) = \begin{cases} \frac{1}{2}\left(1 + \cos\frac{\pi x^2}{{d_0}^2}\right) & \text{if} \quad |x| \leqslant d_0 \\ 0 & \text{if} \quad |x| > d_0. \end{cases} \tag{3.9}$$

The weights thus vanish when $d(L, L_i) \geqslant d_0$. The threshold was experimentally fixed in such a way that about 100 weights do not vanish among the 3000 computed. Vautard (1987) shows that d_0 is the average distance between two fields separated by a 2-day lag. We expect that the composite obtained from the 500 retained days provide a good representation of the large-scale statistics. The ensemble-averaging operator defined this way clearly satisfies the differentiability condition for F. We now turn our attention to the definition of the Euclidian distance. Part I shows that the large-scale variance is concentrated within the second quarter of the channel. It is also shown that this variance is primarily due to vacillations between zonal and blocking regimes. This suggests that the appropriate proximity criterion must be based on the part of the field contained within the second quarter. In addition, since only antisymmetric large-scale solutions are sought, the criterion should involve only the antisymmetric part of the fields. Let us denote the antisymmetric part of the large-scale streamfunction in the upper level (lower level) by ${\psi_L}^1$ (${\psi_L}^2$). The distance between large-scale fields is thus defined as

$$d^2(L, L_i) = \int\int_{D_1} ({\psi_L}^1 - \psi^1_{L_i})^2 dxdy + \int\int_{D_2} ({\psi_L}^2 - \psi^2_{L_i})^2 dxdy, \tag{3.10}$$

where D_1 (D_2) is the upper-level (lower-level) second quarter of the channel. The integrals are actually computed over a finite number of grid points. A grid of 64 $\times$ 20 points is used for fast Fourier transforms (see Part I) and the integrals are computed over the points 17, 18, . . . , 32 in the x-direction and 0, . . . , 20 in the y-direction.

Figure 2 shows a general diagram of the whole procedure. A step of the algorithm can be outlined as follows: Let $L^{(n)}$ be the large-scale field at the nth step of the algorithm. We first compute the distances between $L^{(n)}$ and the L_i's, and select the 5-day periods of proximity ($d(L^{(n)}, L_i) < d_0$). The weights and the composite tendency $T(L^{(n)})$ are then computed. The adjoint operations are performed in order to compute the gradient of $F(L)$ with respect to L (see appendix B). Given $L^{(n)}$, $F(L^{(n)})$ and $\nabla F(L^{(n)})$, the quasi-Newtonian algorithm estimates the next large-scale field $L^{(n+1)}$ which minimizes the cost F in a suitable direction.

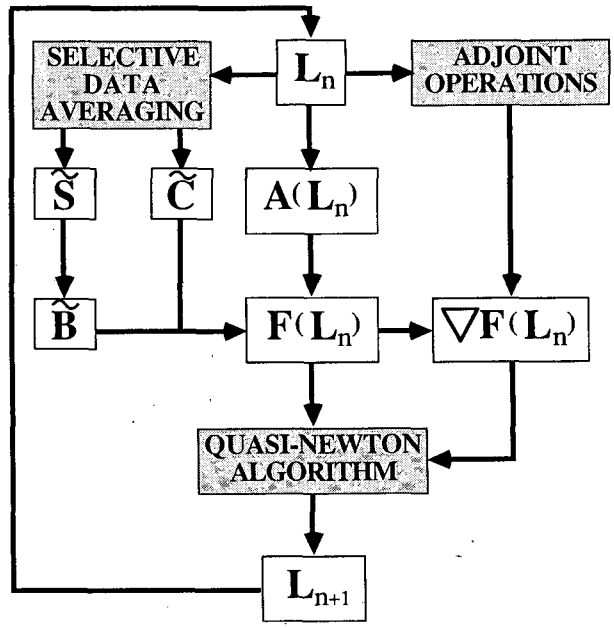

FIG. 2. Sketch of a step of the iterative optimization algorithm. Arrows from one box to another indicate that the source is needed for the computation of the target. The step starts with only knowledge of L_n.

4. Equilibrated regimes

a. Convergence and stability of equilibration

A well-known difficulty of nonlinear optimization is that there is no practical way to systematically explore a phase space whose dimension exceeds a few units (here 14) and to make sure that all solutions have been obtained. Moreover, we expect that by using arbitrary first guesses and a finite dataset, the irregularities of the cost function defined in (3.1) can lead the iterative algorithm to irrelevant local minima where it does not vanish, or even to nonsignificant vanishing minima. Owing to our statistical definition, these latter may be numerous at the periphery of the attractor where the number of observations is small and the fluctuations are large. Relevant solutions may only be obtained in areas where the attractor possesses a high density of trajectories, which drastically reduces the domain to be explored.

As initial conditions for the equilibration we choose a set of 50 5-day means randomly extracted from the 3000 archived. The typical magnitude of the cost F over the 50 points is about 6×10^{15} m^6 s^{-4} and we first iterate the algorithm to reduce F to one-thousandth of this value. After this process, 30 points remain, the other 20 having converged to local minima with $F > 6 \times 10^{12}$ m^6 s^{-4}. The optimization is carried on the former group with a new stop criterion for F at 10^{-8} times the typical value. Only 17 points reach this limit.

Figure 3 shows the projection of the 50 initial conditions (dots), the 30 intermediate states (+) and the 17 convergent solutions (0) onto the plane of the normalized coefficients of the first two EOFs as defined in Part I. Since several cases have merged in the course of optimization, 18 different states are obtained at the intermediate step and seven states as convergent solutions. A clear gathering of the equilibrated states is

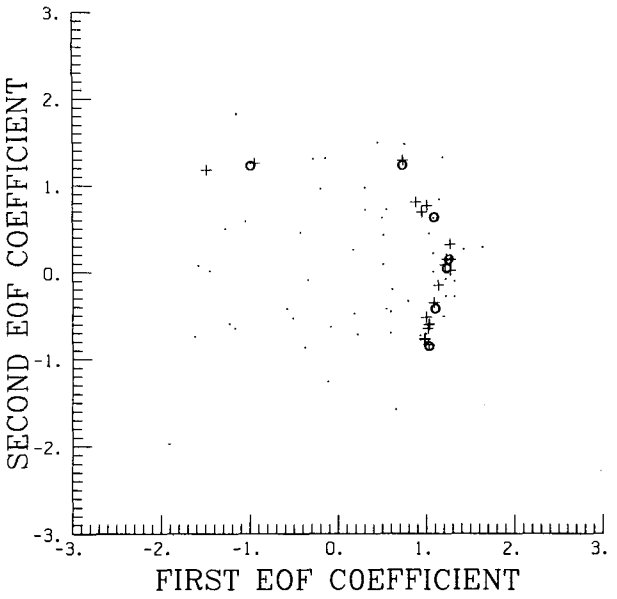

FIG. 3. Projection of the 50 initial conditions (dots) onto the plane of the two normalized first EOF coefficients. Plus signs show the 18 intermediate projections for a cost of 10^{-3} times the typical initial value, and zero signs are the projections of the convergent solutions (10^{-8} times the typical cost).

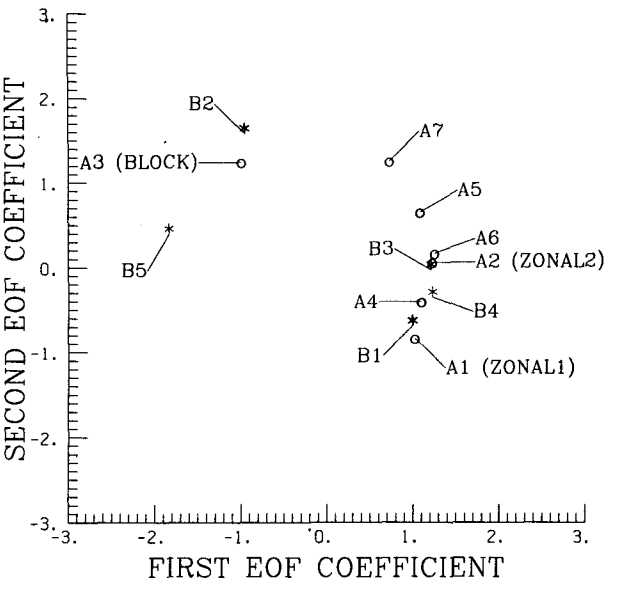

FIG. 4. As in Fig. 3, but for solutions arising from experiment A (A1 to A7) marked with zeros, and experiment B (B1 to B5) marked with asterisks.

visible in Fig. 3, compared to the scattering of the 50 initial points. At the intermediate stage, one group separates with two states (three points) in the second quadrant from a second group with positive first EOF coefficients and characterized by a large scattering of the second EOF coefficient. At the ultimate stage of convergence, one solution remains isolated in the second quadrant while six others are found in the second group. A fast convergence of F towards zero is observed for the seven solutions.

In order to test the significance of the equilibrated solutions, we repeat the same computations with a second independent 15 000-day dataset, originating from the second integration described in Part I. Then, five different solutions are obtained (denoted by B's) which are shown in Fig. 4 together with the solutions obtained from the first dataset (denoted by A's). At first sight there is good agreement between the two datasets in the distribution of solutions which cluster in two separate groups in both cases. But a two-dimensional projection of a 14-dimensional phase space might yield a misleading perception. In order to allow a more quantitative discussion, Table 1 shows the Euclidian distances d between all pairs of solutions shown in Fig. 4. We decide that two solutions do not differ when their distance is less than the threshold d_0 utilized in

TABLE 1. Euclidian local distances d^2 ($\times 10^{-3}$) between pairs of solutions (A1 to A7 and B1 to B5) and between solutions and composites (CB and CZ, see section 5).

	A1 ZONAL1	A2 ZONAL2	A3 BLOCK	A4	A5	A6	A7	B1	B2	B3	B4	B5
A1 ZONAL1	0											
A2 ZONAL2	3.9	0										
A3 BLOCK	19.	15.	0									
A4	1.5	.57	15.	0								
A5	7.2	.65	12.	2.2	0							
A6	4.5	.22	15.	.82	4.7	0						
A7	12.	3.2	8.8	5.7	1.1	2.9	0					
B1	.28	2.2	16.	.53	4.8	2.7	9.1	0				
B2	22.	16.	.32	17.	12.	16.	7.9	19.	0			
B3	3.3	.03	15.	.36	.92	.09	3.7	1.8	16.	0		
B4	2.2	.32	17.	.12	1.8	.48	5.4	1.1	18.	.16	0	
B5	24.	23.	1.9	22.	22.	24.	18.	22.	3.2	23.	25.	0
CB	17.	11.	.58	12.	8.2	11.	5.1					
CZ	1.1	1.3	13.	.25	3.0	1.6	6.3					

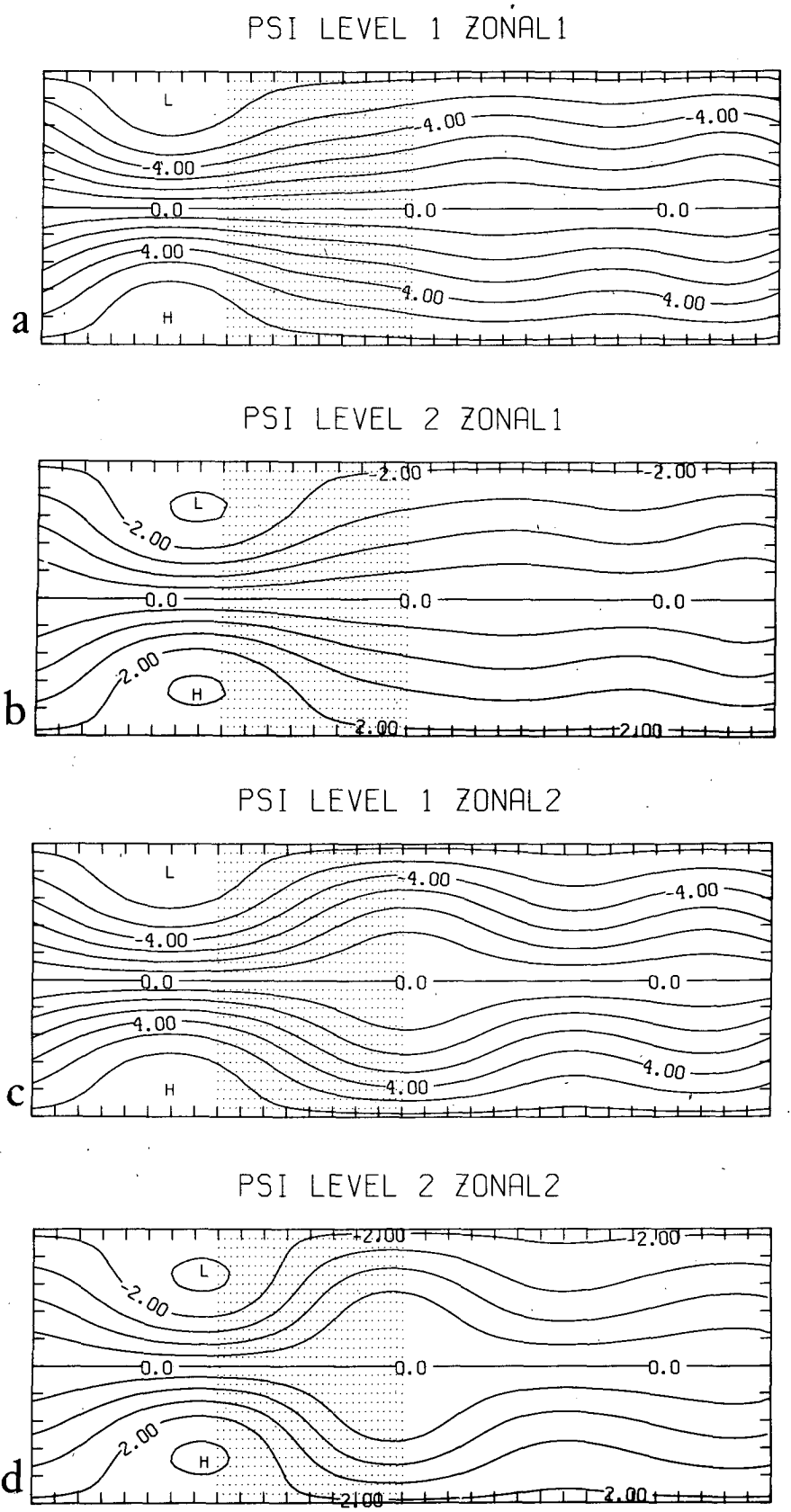

FIG. 5. Streamfunctions associated with the solutions ZONAL1, (a) upper level, and (b) lower level; ZONAL2 (c, d) and BLOCK (e, f). Units are 10^7 m^2 s^{-1}. Dots show the domain used for the computation of the local distance d.

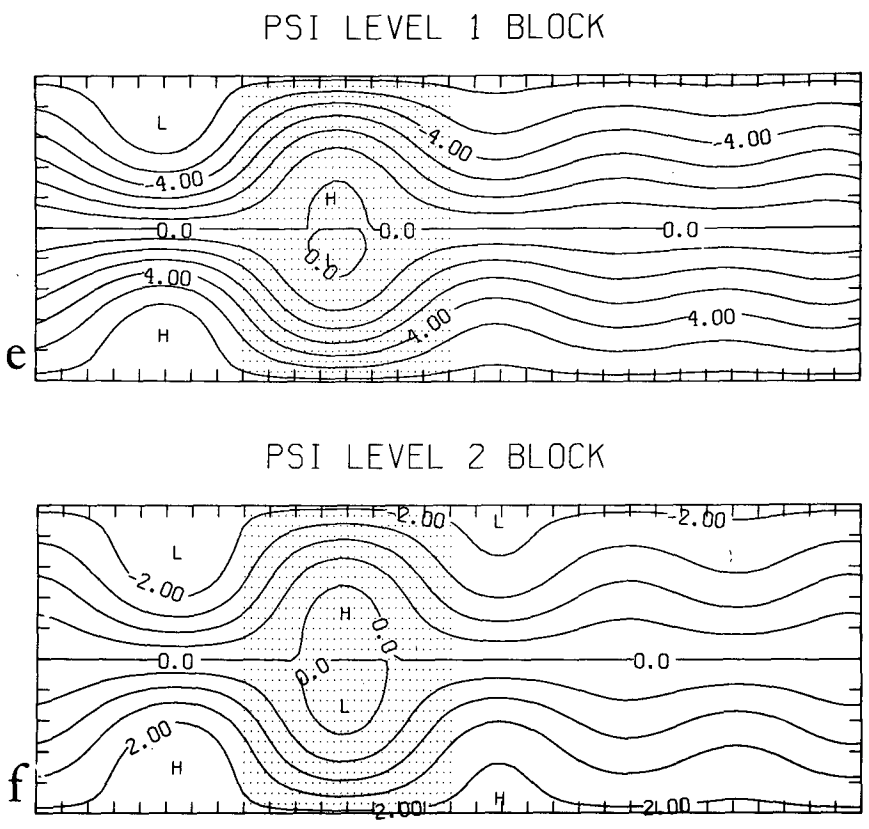

FIG. 5. (*Continued*)

the statistical average, and also that a solution is significant only if there exists a solution obtained from the second dataset within a distance less than d_0. All distances inferior to d_0 are underlined in Table 1, showing that solutions A5, A7 and B5 must be rejected as nonsignificant and that the remaining ones gather into three sets. The first contains A1 and B1. The second is the most crowded with A2, A4, A6, B3 and B4. The third contains only A3 and B3. In addition, one notes that the first two sets are not clearly separated since the distance between B1 and A4 is less than d_0.

b. Solution patterns

Figure 5 shows the spatial patterns of the various groups, A1 (Fig. 5a–b), A2 (Fig. 5c–d) and A3 (Fig. 5e–f). For A1 and A2, the jet extends well downstream from its driven maximum, and particularly for A1, the zonal part of the flow dominates over the wavy part; we refer to these solutions as ZONAL1 and ZONAL2. However, A3 displays a marked wavy structure at the exit of the jet; thus, we refer to it as BLOCK since its dipolar structure is reminiscent of the North Atlantic blocking pattern. The presence of closed cells indicates that the anomaly is strong enough to produce easterlies at the central latitude as observed during blocking events over western Europe. The three patterns do not differ significantly in the first quarter of the channel, suggesting that the shape of the jet alone does not determine the structure of the exit region.

Differences between patterns are well marked within the second quarter, and particularly in the lower layer. For ZONAL2, the exit of the jet displays a diffluent structure centered near the middle of the channel. This is not the case for ZONAL1 where the flow remains almost parallel. The anomaly patterns (not shown) for ZONAL1 and BLOCK exhibit maximal amplitudes slightly downstream from the regions of maximum variance (see Fig. 12 of Part I). The block is centered at the longitude where the number of closed-cell blocking events is found to be maximum. ZONAL2 is associated with a positive anomaly in the northern part near the central longitude of the channel and a negative anomaly at the exit of the basic jet, complemented by their images in the southern part. These anomalies are not strong enough to produce easterlies. The weak wavy structure observed in the second half of the channel for all solutions is presumably due to the small number of large-scale modes involved.

BLOCK has a barotropic structure with almost in-phase upper and lower layers while for ZONAL1 and ZONAL2, the upper-layer jet maximum is tilted westward with respect to the lower layer, an indication that the energetics might be different in the two cases. Actually, this tilt is also seen for the time-average field

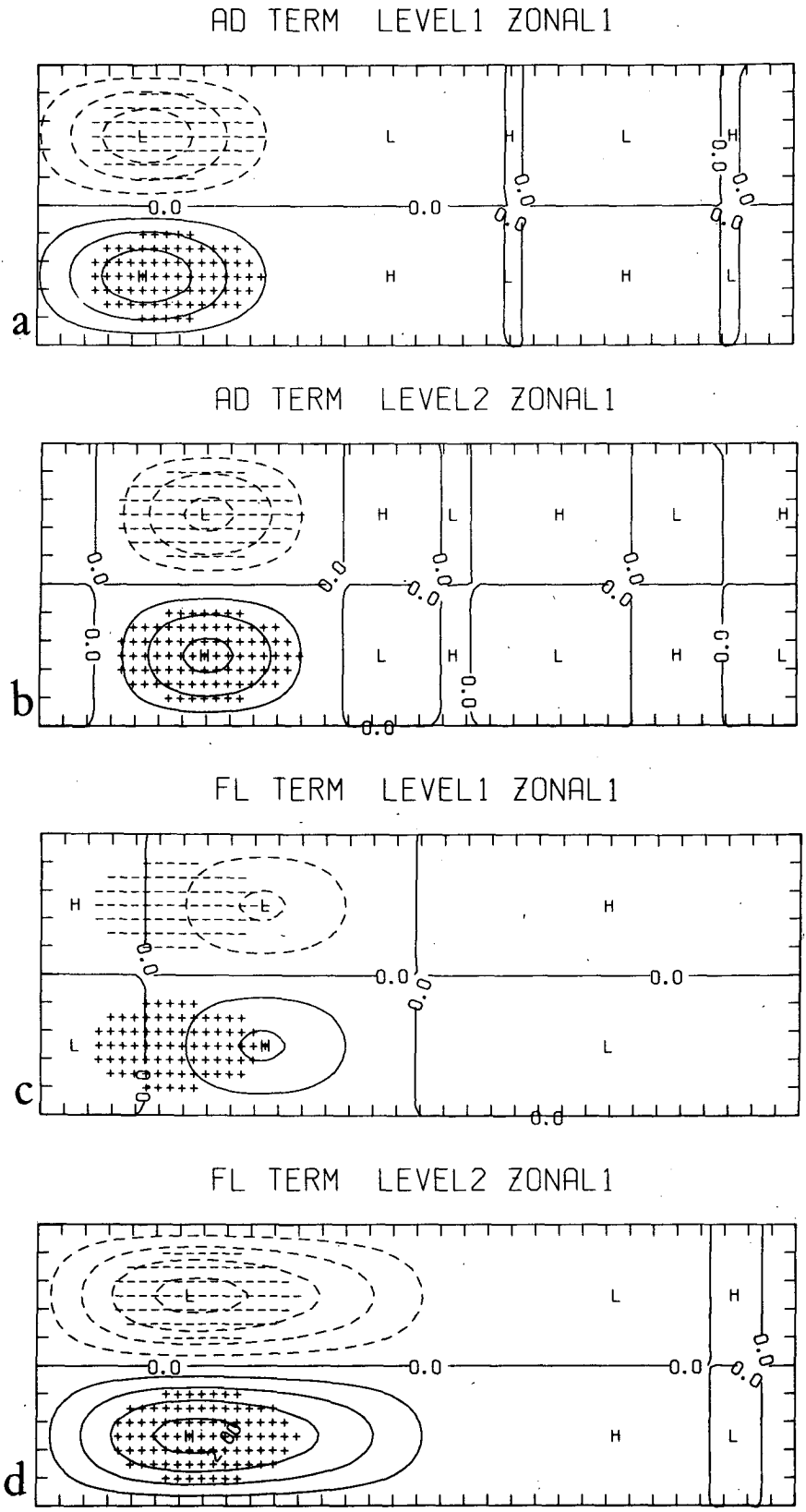

FIG. 6. The total advection term *AD* and flux term *FL* (contours) in the two layers for ZONAL1 and BLOCK, after linear transform $q \rightarrow \psi$. Units are 10 $m^2\ s^{-2}$. Contour interval is 10 $m^2\ s^{-2}$ in the upper layer and 5 $m^2\ s^{-2}$ in the lower layer. Negative contours are dashed. The areas filled with plus symbol are the areas where the corresponding streamfunction anomaly is positive and exceeds $1 \times 5\ 10^7\ m^2\ s^{-1}$ for the upper layer and $0 \times 7\ 10^7\ m^2\ s^{-1}$ for the lower layer. Areas

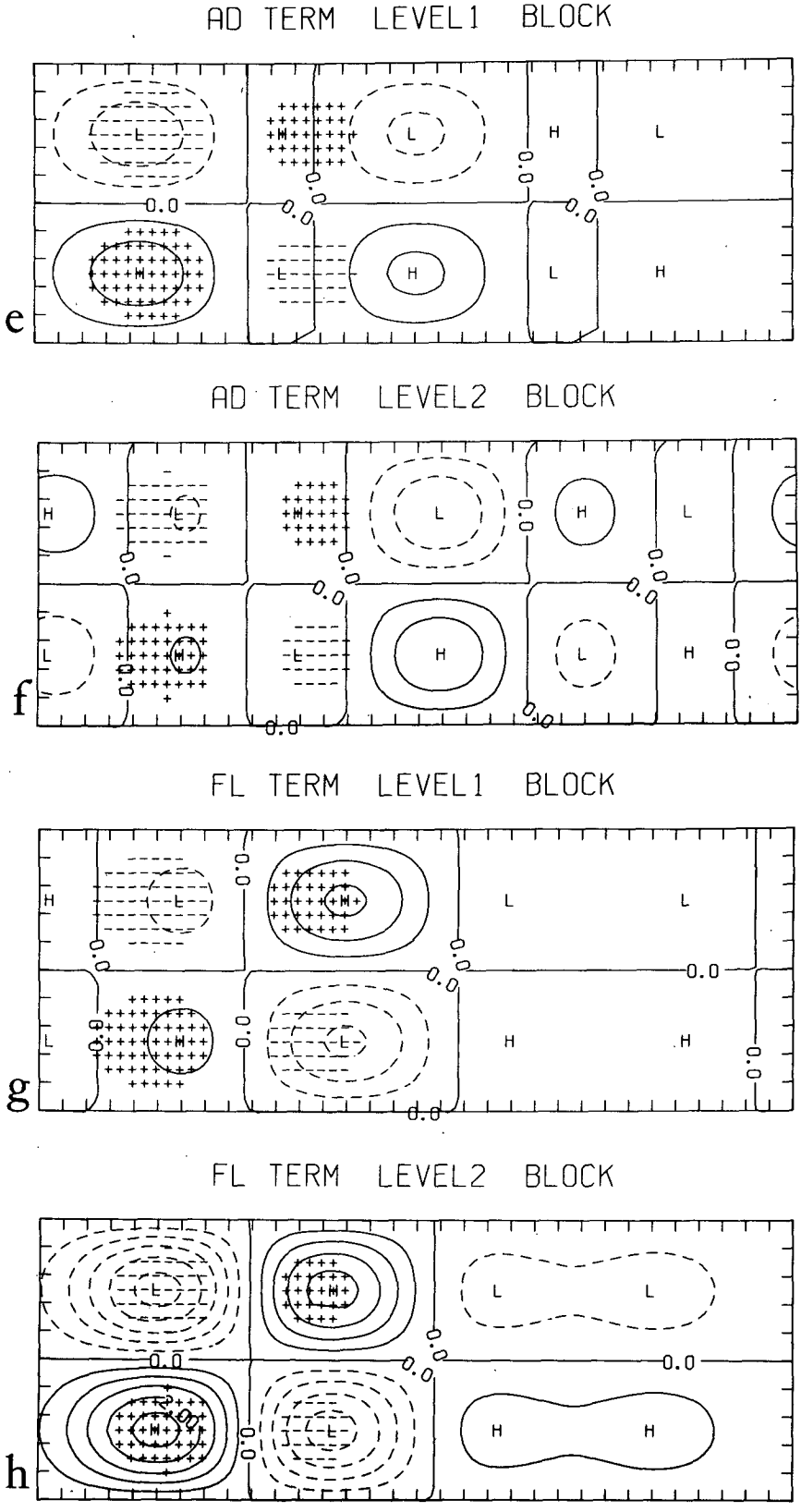

filled with minuses are the same for negative anomalies. The *AD* (*FL*) terms for ZONAL1 are shown in a, b (c, d) in the two layers (a: upper, b: lower, c: upper, etc.), and e, f, g, h are the corresponding maps for BLOCK.

(see Fig. 5 of Part I), and is also observed in the atmospheric mean flow (Oort 1983). The baroclinity is strongly reduced in the three solutions with respect to the basic flow ψ^*: in the ZONAL1 and BLOCK cases, the maximum shears are 29 and 24 m s^{-1}, respectively, instead of 37 m s^{-1}.

c. *Balance of equilibrated solutions*

We have, so far, spent a lot of effort in incorporating the transient effects in the equilibration problem. It is thus important to assess a posteriori whether or not this effort was necessary. The simplest method of assessment is to go through the detailed description of the various contributions involved in the statistical equilibration of the two solutions ZONAL1 and BLOCK. Apart from some minor differences, the conclusions of what follows for ZONAL1 also apply to ZONAL2. In order to discuss more physical quantities than the terms A, B and C of Eq. (2.3), we group the terms as follows:

$$T(L) = G + AL + AN + DI + FL. \quad (4.1)$$

Here, G is the constant large-scale part of the forcing term; and AL and AN group, respectively, the linear and the nonlinear part of the mean advection. More precisely, if ${q_1}^L$, ${q_1}^S$, ${\psi_1}^L$ and ${\psi_1}^S$ are the large- and small-scale parts of the vorticity and the streamfunction in the upper layer, the upper-layer terms AL_1 and AN_1 are given by

$$AL_1 = -U_1 \frac{\partial {q_1}^L}{\partial x} - [\beta + R_1^{-2}(U_1 - U_2)] \frac{\partial {\psi_1}^L}{\partial x}, \quad (4.2)$$

$$AN_1 = J^L({q_1}^L + \overline{{q_1}^S}, {\psi_1}^L + \overline{{\psi_1}^S}), \quad (4.3)$$

where J^L denotes the projection of the Jacobian operator onto the large-scale modes.

In (4.1), DI groups all the linear dissipation terms acting on the large-scale flow, and FL is the transient part of the feedback of the small scales onto the large scales:

$$FL_1 = \overline{J^L({q'_1}^S, {\psi'_1}^S)} \quad (4.4)$$

where the primes denote the deviations from the ensemble average (overbar). Here, FL slightly differs from C by removing the small contribution $J^L({q_1}^S, {\psi_1}^S)$ of the mean small scales, now included in the mean advection term AN; $\overline{{\psi_1}^S}$ weakly depends on the large-scale flow and closely resembles the small-scale part of the mean flow averaged over the whole integration. The self-coupling $J^L(\overline{{q_1}^S}, \overline{{\psi_1}^S})$ is small compared to other terms but the mixed couplings involved in term B are significant. Since the term $J^L({q_1}^L, {\psi_1}^L)$ vanishes identically, owing to our choice of large-scale truncation, AN is close to B. We finally group the advection terms and the forcing G (smaller than the former terms) in the *total advection* AD:

$$AD = G + AL + AN. \quad (4.5)$$

The sum $AD + FL + DI$ vanishes for equilibrated solutions, so that we only need to consider the AD and FL contributions. Figure 6 shows these quantities for the two solutions ZONAL1 and BLOCK, in terms of their associated streamfunction field. More precisely, the transformation $q \rightarrow \psi$ is applied before drawing, in such a way that we can directly discuss the balance of the streamfunction fields shown in Fig. 5 (see also section 4 of Part I).

In ZONAL1, the advection AD clearly acts to maintain the jet in both layers since its pattern almost coincides with the anomaly pattern of the solution. In the upper layer, the main in-phase component of AD is provided by the linear advection AL, while in the lower layer the main contribution is from the forcing G. The FL term tends to propagate the jet downstream in the upper layer, while in the lower layer it appears to both propagate and reinforce the jet. Consequently, baroclinity also tends to be reduced by FL since small-scale baroclinic perturbations extract potential energy from the large-scale flow. Baroclinity is restored by AD but an overall higher contribution is needed in the lower layer to balance the Ekman damping.

A very different situation arises in BLOCK. In this case, the jet is maintained by AD in the upper layer and by FL in the lower layer. A similar contribution is given by the three components of AD to the in-phase component of the upper layer. The baroclinity is again destroyed by FL and restored by AD, with a higher contribution in the lower layer as in ZONAL1. The most important result concerning the blocking is that the transient feedback FL plays a crucial role in the maintenance of the blocking dipole in the BLOCK case. It acts mainly against dissipation in both layers, but a significant downstream shift is observed in the upper layer to balance advection. The FL term is able to regenerate the dipole within 7 days in the upper layer and 4 days in the lower layer, thus showing that the solution is strongly forced. Note also that AD weakly contributes to the block itself but tends to reinforce the downstream confluence.

We have also performed the same analysis on the large-scale mean flow (for which the tendency does not vanish, as mentioned in section 4a) and the results (not shown here) are qualitatively similar to those obtained for ZONAL1. The statistical tendency, even though rather small, induces a bias towards reinforcement and downstream extension of the jet.

As a final remark, we emphasize that the above results are very stable. They are almost identically recovered using the second 15 000-day dataset.

d. *Variability of the balance terms*

The previous results suggest that the BLOCK regime separates from ZONAL1 and 2 and from the mean

flow. Not only is it separated in space (Fig. 4) but it occurs less often than the zonal counterparts. (With the same offset $d_0^2 = 6 \times 10^{-4}$, 99 analogs were selected for BLOCK, 167 for ZONAL1 and 171 for ZONAL2.)

In order to measure the variability of the feedback terms, we define the moments of B and C in terms of the energy norm:

$$m_1^2(B) = \langle B, B \rangle, \quad m_1^2(C) = \langle C, C \rangle, \quad (4.6)$$

$$m_2^2(B) = \sum_{i=1}^{3000} w(L, L_i) \langle B(L, S_i), B(L, S_i) \rangle,$$

$$m_2^2(C) = \sum_{i=1}^{3000} w(L, L_i) \langle C_i, C_i \rangle, \quad (4.7)$$

and the variances

$$\sigma^2(B) = m_2^2(B) - m_1^2(B),$$

$$\sigma^2(C) = m_2^2(C) - m_1^2(C). \quad (4.8)$$

Thus the ratios

$$D(B) = \frac{\sigma^2(B)}{m_1^2(B)}$$

and

$$D(C) = \frac{\sigma^2(C)}{m_1^2(C)} \quad (4.9)$$

provide a measure of the relative dispersion of the 5-day means. The values of these quantities for ZONAL1 and BLOCK are given in Table 2. We have also calculated as reference figures the corresponding values for the mean flow and the global moments (without weighting) over the whole experiment (for C only). By comparing the moments of the mean flow and the global moments, it is readily seen that the estimation of the mean small-scale feedback with selective averaging—about 200 situations are selected for the mean large-scale flow—is close to the globally averaged value. However, one sees that ZONAL1 is more likely to behave as the mean flow than BLOCK. The dispersion and the variance are greater in BLOCK than in ZONAL1 for the B term, while for the C term, the dispersion in the ZONAL1 and the mean flow case is almost the double that of the BLOCK case. BLOCK again appears as a rather well-defined isolated regime while ZONAL1 behaves more like a continuum, as it exhibits a spreading of small-scale activity comparable to the mean flow. The mixed term B is less sensitive than C to the large-scale flow. It has already been noted that the stationary small-scale part of the flow which leads to B is not dependent on the regime.

5. Persistence and equilibration

As pointed out in section 3, the equilibration method, based on the balance of the statistical tendency, does not a priori yield any information about persistence of the balanced large-scale patterns. However, if the flow exhibits systematically persistent patterns, confined within narrow regions in phase space, such patterns should yield to small statistical tendencies. In other words, recurrent persistent patterns are solutions of the equilibration problem while the opposite is not necessarily true.

In Part I, we analyze the persistence properties of the flow using a score based on the behavior of 15-day sequences (see section 5 of Part I). Given the choice of an offset score, s_0, a set of persistent sequences is defined and the histogram of the EOF coefficients of this population is computed. A highly non-Gaussian distribution of persistence is found although no multiple maxima emerge. Dividing the histogram of persistent data by the histogram of the whole set of data gives the probability distribution of persistence as a function of the large-scale flow characteristics. This distribution, shown in Fig. 7 (same as Fig. 19a of Part I), is far from being uniform and exhibits two distinct maxima. This result is a consequence of the fact that preferred flows exist for persistence though they are relatively rare, so that no separated maxima occur in the raw histogram. Figure 7 also shows the positions of the equilibrated solutions for the two analyzed datasets considered here. There is a clear relation between the significant solutions found in section 4 and the regions of maximal probability of persistence. In particular, the points representing BLOCK and ZONAL1 solutions are found very close to the two maxima. Persistent sequences crossing the dotted areas of Fig. 7 are composited respectively in Figs. 20 and 21 of Part I. These two composites closely resemble BLOCK for the

TABLE 2. Moments and dispersion of terms B and C. The moments are normalized by the standard value of F: 6.125×10^{15} m^6 s^{-4}.

	$m_1^2(B)$	$m_2^2(B)$	$\sigma(B)$	$D(B)$	$m_1^2(C)$	$m_2^2(C)$	$\sigma^2(C)$	$D(C)$
ZONAL1	2.8	3.6	0.8	0.3	2.3	5.9	3.7	1.6
BLOCK	2.6	4.0	1.4	0.5	3.4	6.3	3.0	0.9
Mean flow	1.8	2.5	0.6	0.3	2.3	6.7	4.4	1.9
Global	/	/	/	/	2.0	6.4	4.4	2.2

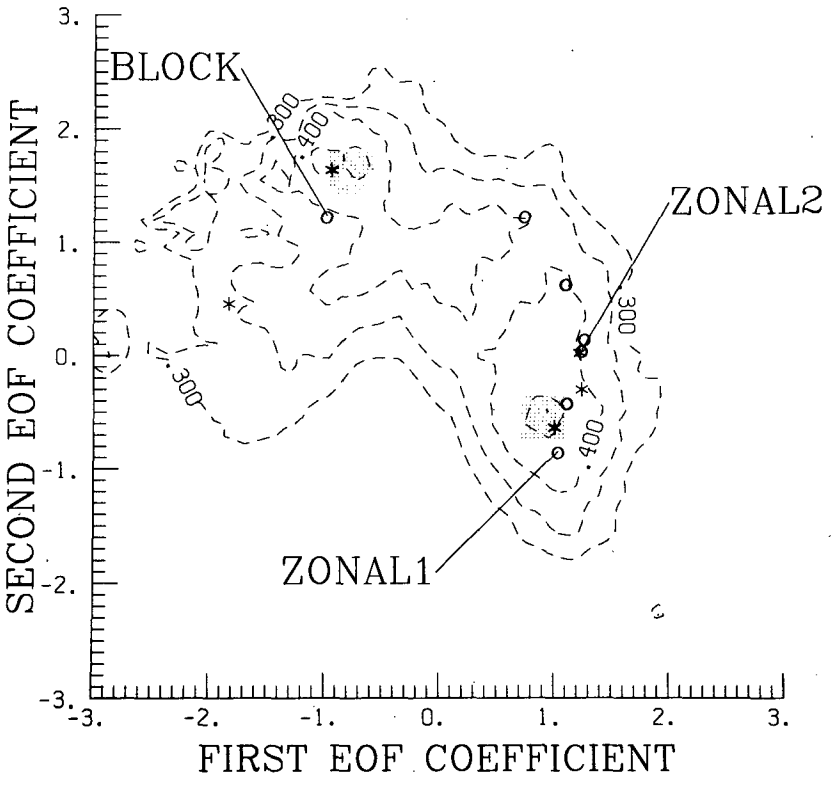

FIG. 7. Contours of the persistence probability (dashed lines) in the same projection as in Fig. 3 and 4. For details, see the text in Part I. Contours shown are 0.30, 0.35, 0.40, 0.45. Dotted areas are used for compositing persistent blocking (second-quadrant) and zonal (fourth-quadrant) sequences. The solutions of the equilibration are superimposed with the same symbols as in Fig. 4.

first (CB) and ZONAL1 for the second (CZ), although the amplitude of the blocking dipole in CB is somewhat smaller than in BLOCK. We attribute the discrepancy to the definition of the blocking periods of Part I which run from the onset to the end of the phenomena though here we only deal with well-established structures. The local distances between CB, CZ and equilibrated solutions are reported in Table 1. The distance between CB and BLOCK and between CZ and ZONAL1 is less than the threshold d_0.

Another way to establish the relation between persistence and equilibration is to compare directly the 5-day periods selected for the BLOCK and ZONAL solutions with the persistent 15-day periods. For this purpose, we use only the first 15 000-day dataset. We denote as P_i the 15-day period beginning at day i which corresponds to a score s_i of persistence [the lower the score, the more persistent the sequence, (see Part I)]. The scores are sorted into ascending order, so that the sorted periods have scores satisfying

$$s'_1 < s'_2 < \ldots < s'_j \ldots .$$

Among the 3000 5-day large-scale averages L_k we choose the patterns for which $d(L, L_k) < d_0$, where L is either BLOCK or ZONAL1. For each 5-day period U_k, we consider all the overlapping 15-day sequences (they can overlap over 1, 2, . . . , 5 days), and we associate U_k to the most persistent of these latter, i.e., the one with the lowest score s. In this way, a one-way correspondence table between 5-day and 15-day periods can be set up. This correspondence is described by a function h such that $h(U_k) = P'_j$.

Then, we count the number of periods U_k having an h-image ranked among the n most persistent P_j's, and denote it by $K(n)$; $K(n)$ thus provides a good idea of the persistence quality of the periods during which the large-scale flow resembles to L. The smaller n, the more persistent the sequences are. (Note that the value d_0^2 is twice that of the threshold previously used, a necessary feature in order to get significant figures.)

In the BLOCK case, 280 5-day periods are extracted, and 358 in the ZONAL1 case. In order to see whether these periods are significantly more persistent than a "random" selection of 5-day periods, we perform a Monte-Carlo calculation that estimates the "normal" values of $K(n)$. More precisely, for BLOCK, 100 tests are performed using 280 randomly chosen 5-day periods, and $K(n)$ is computed for each test. The 100 evaluations of $K(n)$ are sorted and the 5th and the 95th values are taken as the bounds of the 90% con-

fidence interval. The same procedure is applied to ZONAL1, now using 358 random periods for each test. Figures 8a and 8b show $K(n)$ for ZONAL1 and BLOCK, together with the 90% confidence interval (shaded area). In both cases, the curve lies above the confidence interval, confirming that the local distance d selects more persistent sequences in the vicinity of the equilibration solutions than a random choice. It is noteworthy that for BLOCK, the curve enters the confidence interval near $n = 4000$, indicating that there are relatively less persistent periods than for the zonal case, but they are well ranked with the persistence criterion, while for the zonal case, the persistence quality of the periods is less since the difference between $K(n)$ and its normal value is larger and maximal near $n = 4000$. We can conclude that blocking events are very steady but they do not occur as often as zonal regimes.

The score used here and in Part I takes into account the flow within the whole channel. Two other scores are used in Vautard (1987) based on local persistence properties, both of them giving a curve which falls within the confidence intervals for BLOCK, but not for ZONAL1. This is an additional argument for the choice made in Part I.

It may finally seem paradoxical that a local proximity criterion has to be used for equilibration and a global proximity criterion for persistence, yielding similar results. Indeed, the equilibrated solutions are rather insensitive to a variation of the domain used for the proximity criteria. Close solutions may be obtained with a global proximity criteria but at the price of compositing a lower number of cases, and thus with a lower statistical significance. We also remark that though the proximity criterion is local, the equilibration is performed over the whole channel. A final reason is that no temporal filtering is applied prior to persistence calculations, rendering the local structure analysis sensitive to high-frequency noise.

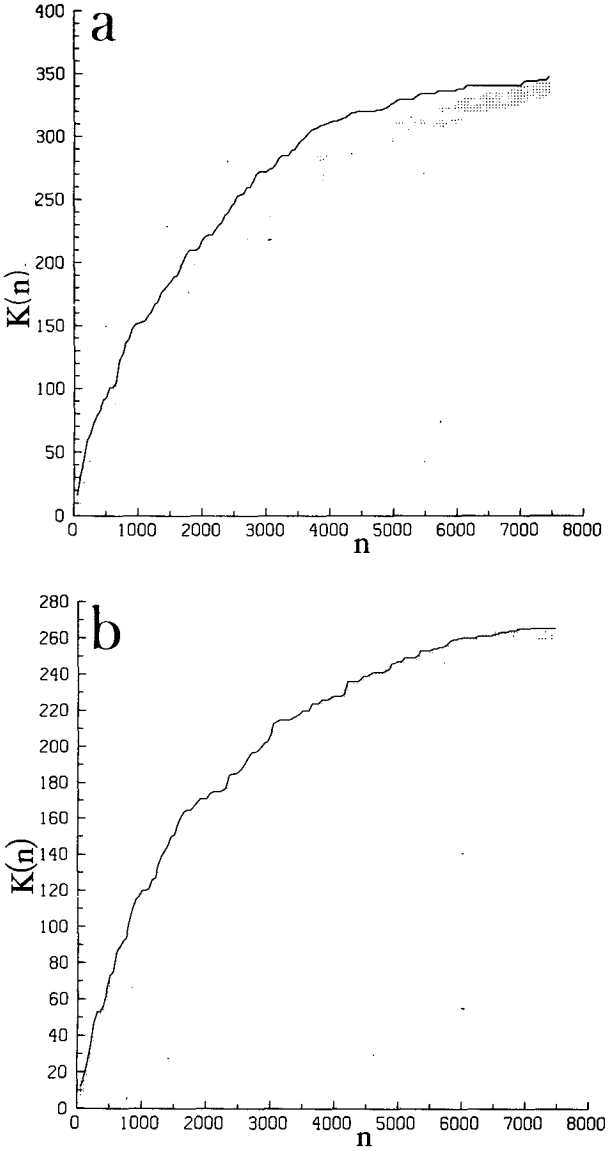

FIG. 8. Plot of $K(n)$ against n for (a) ZONAL1 and (b) BLOCK together with the 90% confidence intervals (dotted area). See text for definitions.

6. Linear parameterization of transients

Here we consider the evolution of small amplitude perturbations superimposed with the large-scale patterns of ZONAL1 and BLOCK. The purpose is to compute the feedback and the secondary circulation induced by the most unstable mode and to compare them with the diagnosed transient feedbacks and the equilibrated solutions. In other words, we test how a quasi-linear theory, as Reinhold and Pierrehumbert (1982) use, can parameterize the observed transients during the equilibrated regimes. The linearized prognostic equations read

$$\frac{\partial q_1'}{\partial t} + U_1 \frac{\partial q_1'}{\partial x} + (\beta + R_1^{-2}(U_1 - U_2)) \frac{\partial \psi_1'}{\partial x} + J(\psi_1', \tilde{q}_1) + J(\tilde{\psi}_1, q_1') = E_1' \quad (6.1a)$$

$$\frac{\partial q_2'}{\partial t} + U_2 \frac{\partial q_2'}{\partial x} + (\beta + R_2^{-2}(U_1 - U_2)) \frac{\partial \psi_2'}{\partial x} + J(\psi_2', \tilde{q}_2) + J(\tilde{\psi}_2, q_2') = E_2', \quad (6.1b)$$

where the primes denote perturbation fields and the tilde denotes one of the large-scale fields ZONAL1 or BLOCK.

The eigenvalues and eigenmodes of Eqs. (6.1a) and (6.1b) are computed in the same way as in Part I for the basic field ψ^*. Comparing with the unstable mode of the basic flow ψ^*, it can be shown (Vautard 1987) that significantly fewer unstable modes are observed for BLOCK and ZONAL1 than for ψ^*; the greatest

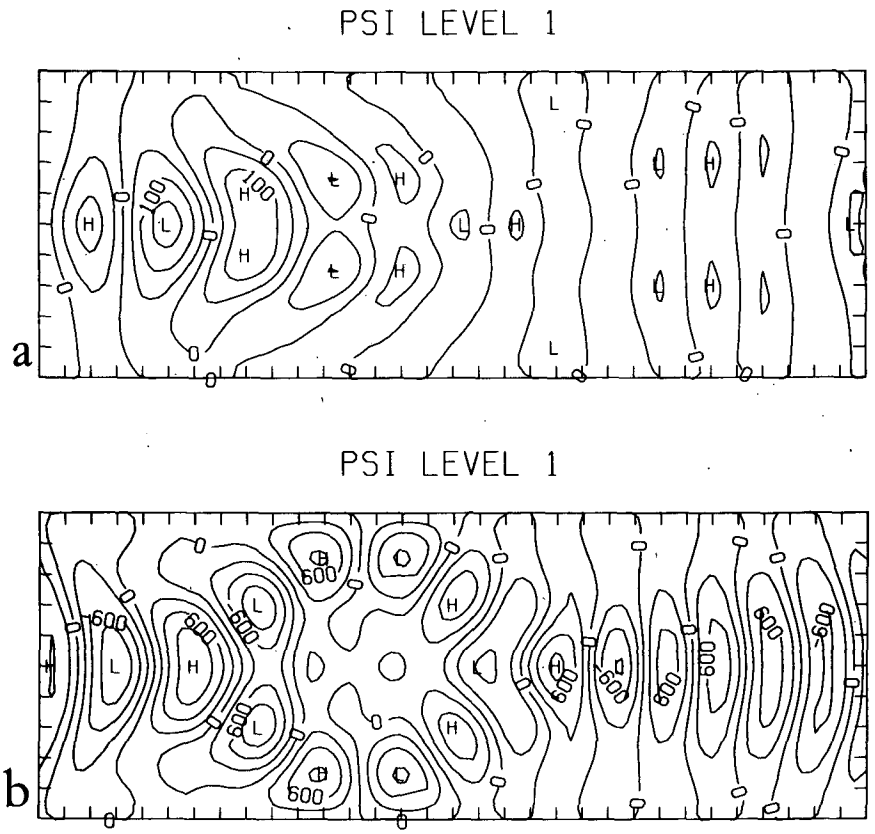

FIG. 9. Instantaneous chart of the upper-layer streamfunction contours (arbitrary amplitude) for the first unstable eigenmode of (a) ZONAL1 and (b) BLOCK.

growth is also less for the two former than for the latter. This result is not surprising since the maximum shear for BLOCK and ZONAL1 is significantly weaker than for ψ^*. The other important discrepancy lies in the existence of a barotropic unstable stationary eigenmode for the basic field, whereas neither unstable or marginally stable such eigenmodes are present for BLOCK and ZONAL1. In Part I, it has been shown (section 4) that this mode accounts for the difference between ψ^* and the observed mean flow.

Figure 9 shows an instantaneous chart of the upper-layer perturbation streamfunction for the most unstable modes of ZONAL1 and BLOCK. Counting the number of waves, an average zonal wavenumber 7 is measured in longitudinal direction. Figure 10 shows the associated variance charts together with the phase gradients (arrows), computed as in Part I, which point towards the local direction of propagation and have an amplitude proportional to the local wavenumber. Local propagation lines roughly follow the isopleths of ZONAL1 and BLOCK streamfunctions (see Figs. 5a and 5c) except at the exit of the jet and at the lateral boundaries where the local longitudinal wavelength decreases dramatically leading to wave absorption. It is also noteworthy that near the maximum of the jet, arrows are twice as short as those in the second half of the channel, but as pointed out in Part I, this is not surprising since the zonal wind doubles within the jet (and the phase speed is larger), while the period is fixed. In both cases, the local wavelength turns out to be about 5000 km in this region. The scattering structure of the phase gradients within the center of the BLOCK shows that there is no propagation within this region but rather that the eddies turn around the block.

The storm-track structure of the variance in ZONAL1 differs considerably from the splitting of the variance in BLOCK. The maximum amplitude of the eigenmode is observed within the splitting region in the latter case while it is located relatively upstream in ZONAL1. In Fig. 10b, the perturbations weaken during the first part of their course around the block, but do not weaken after, and a second maximum of the variance occurs in the second half of the channel. This marks a noticeable difference with the results of Shutts (1983), who shows that almost all the energy of the eddies is contained upstream from the blocking region. Since our vertical wind shear is globally unstable, baroclinic perturbations draw their energy from available potential energy of the mean shear all along the channel.

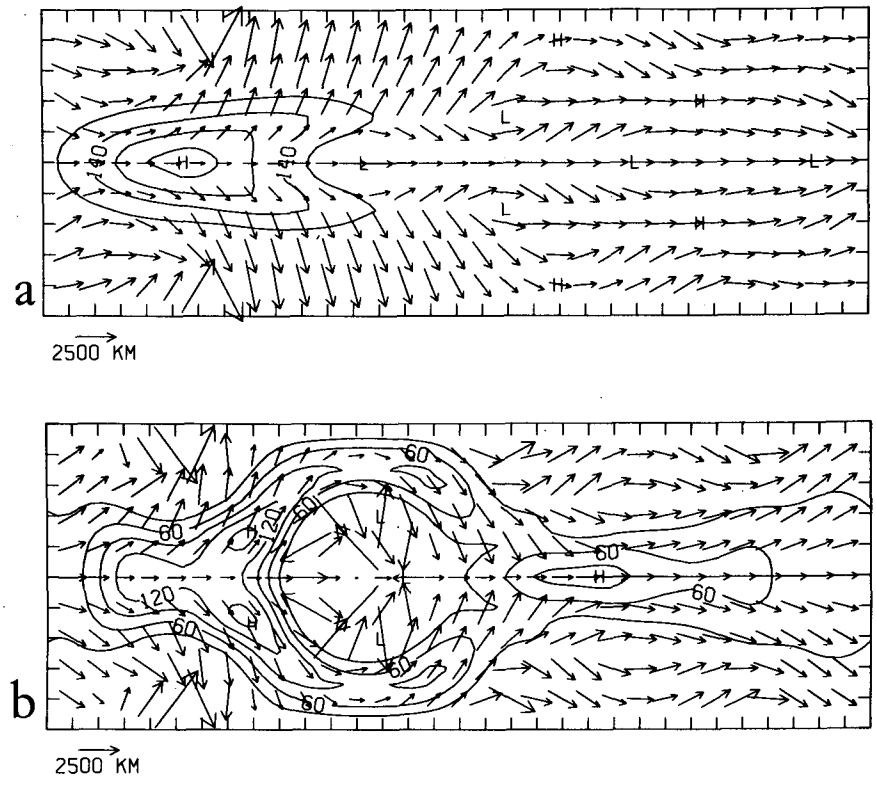

FIG. 10. Upper-layer streamfunction variance contours (arbitrary amplitude) for the first unstable eigenmode of (a) ZONAL1 and (b) BLOCK together with phase gradients. The reference arrow indicates a phase gradient (local wavenumber) corresponding to a wavelength of 2500 km.

However, it can be shown that as eddies propagate downstream, they become less baroclinic. Simmons and Hoskins (1978) associate this behavior with the mature stage of the life cycle of nonlinear baroclinic disturbances, and Pierrehumbert (1984) recovers it through linear analysis of a nonparallel flow as well.

We now compare the feedbacks of the most unstable eigenmodes onto the large-scale patterns, with the previously calculated nonlinear forcings (section 4c). Figure 11 shows the contribution $J(\psi', q')$ (averaged over a cycle) for the most unstable eigenmodes of ZONAL1 and BLOCK, plotted after conversion to streamfunction, and with an arbitrary amplitude. The contribution of the large-scale part of the eigenmode (which is not removed here) is found to be negligible. Figure 11 shows all scales of the feedback; in Fig. 12, large-scale filtering has been applied and we retain only the feedback onto the L modes. The latter can be directly compared with the FL terms shown in Fig. 6c and 6g. Rather good agreement is observed in the ZONAL1 case in the upper layer between Fig. 12a and 6c. This is also true for the lower layer and confirms that in this case linear theory gives a good account of the transient feedback. Contrarily, Figs. 12b and 6g strongly differ in the BLOCK case: the two patterns are out of phase. Furthermore, a computation, performed as in Shutts (1983), of the secondary flow induced by the pattern 12b shows a well-marked quadrupole structure but located downstream from its position in BLOCK. In this case, the fully nonlinear dynamics is not correctly approximated by linear theory and the prognostic parameterization of transients appears as a very difficult challenge. Since several unstable modes merge with comparable e-folding times, one may think that a proper combination of these latter may give the right feedback. The difficulty is that we do not know any way to predict a priori this combination. One may add that certain initial configurations can lead to quickly growing instabilities, much faster than the most unstable eigenmodes (Reinhold 1986; Weng and Barcilon 1987).

7. Concluding remarks

The statistical–dynamical method introduced in this paper provides a quantitative definition of quasi-stationary weather regimes based on an ensemble-average balance of large-scale dynamics. It incorporates the feedback of transients which may themselves depend nonlinearly on the large-scale flow. Their dependence is diagnosed from an observation dataset and is put in the form of a continuous functional relationship used

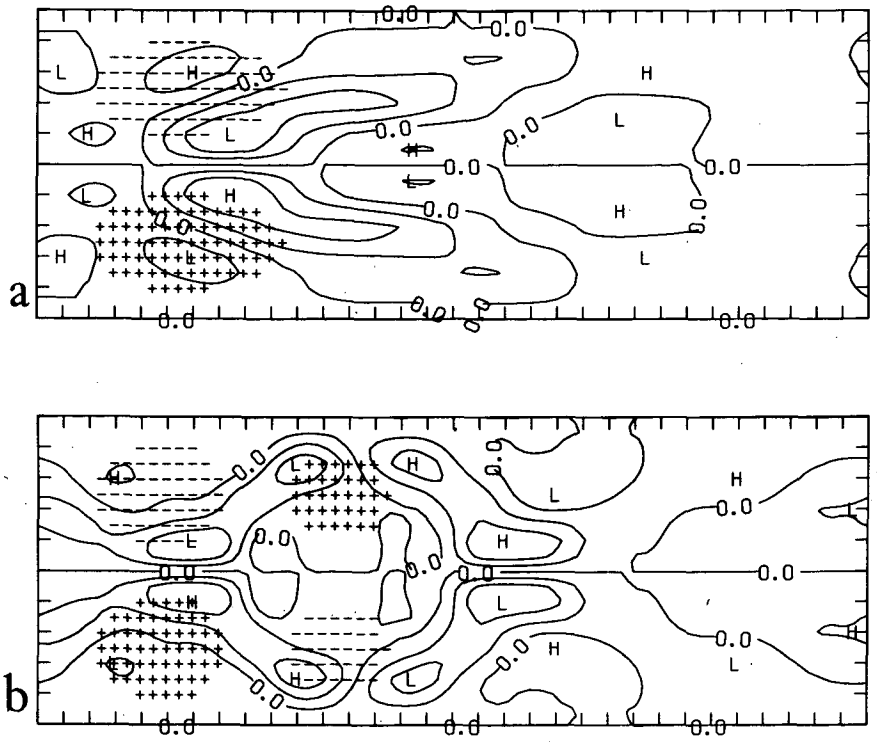

FIG. 11. Time-average (over a cycle) of the nonlinear feedback $J(q', \psi')$ after $q \rightarrow \psi$ transform, in the upper layer for (a) ZONAL1 and (b) BLOCK. Areas filled with plus and minus symbols are the same as in Fig. (6c) and (6g). Arbitrary units.

to close the statistical–dynamical stationary equation satisfied by the large-scale flow. We apply the method to a quasi-geostrophic baroclinic model with locally enhanced shear and we detect several regimes falling within two families of zonal and blocking types respectively. The blocking regime corresponds to a well-defined pattern that appears to be particularly robust to variations in the dataset or in the initial guess. However, the zonal regime does not possess a single pattern but rather corresponds to an ensemble (a continuum?) of solutions elongated in phase-space along the direction of the second EOF which modulates the diffluence of the flow downstream from the jet. In both zonal and blocking regimes, the transients are an important factor of the maintenance of the large-scale flow. In the blocking case, the anomalous dipole is mainly maintained by the transients against dissipation. We show that in the zonal case, dynamics is largely governed by linear and quasi-linear mechanisms but that fully nonlinear mechanisms are crucial to account for the maintenance of the blocking flow. The quasi-stationary solutions are also in good agreement with the composite regimes of maximal probability of persistence, independently defined from a pure diagnostic approach.

Although based on an objective ground, the method still possesses in its present shape several arbitrary settings. The diagnosed dependence of transient fluxes on the large scales is a priori sensitive to the way analogs are defined. But since high amplitude persistent anomalies mainly occur within the second quarter of the channel, all measures of similarity giving a significant weight to this domain lead to similar results. More serious difficulties arise from the scale separation that we have adopted for the sake of easiness. Undoubtedly, the spatial-temporal analysis (cf. Part I) on which the separation is based does not provide an unambiguous prescription. An effect is that when large scales are defined with an insufficient number of degrees of freedom, the optimized solutions may be combinations of separated regimes. In the other extreme, when the number is too large, the search for analogs leads to very poor subsets, on the one hand, and the inclusion of fluctuating scales leads to nonpersistent solutions, on the other. In the present study, we have removed these ambiguities by a comparison with an independent diagnostic study of persistence properties.

However, the orthogonality of transients and large-scale flow is only a matter of technical convenience. At the price of an additional amount of complexity, this assumption can be removed. Another prominent problem is the fact that Fourier modes are in no way the best functional basis to represent the quasi-stationary structure of the flow. Accordingly, we may expect to improve the analysis by using, for instance, the large-

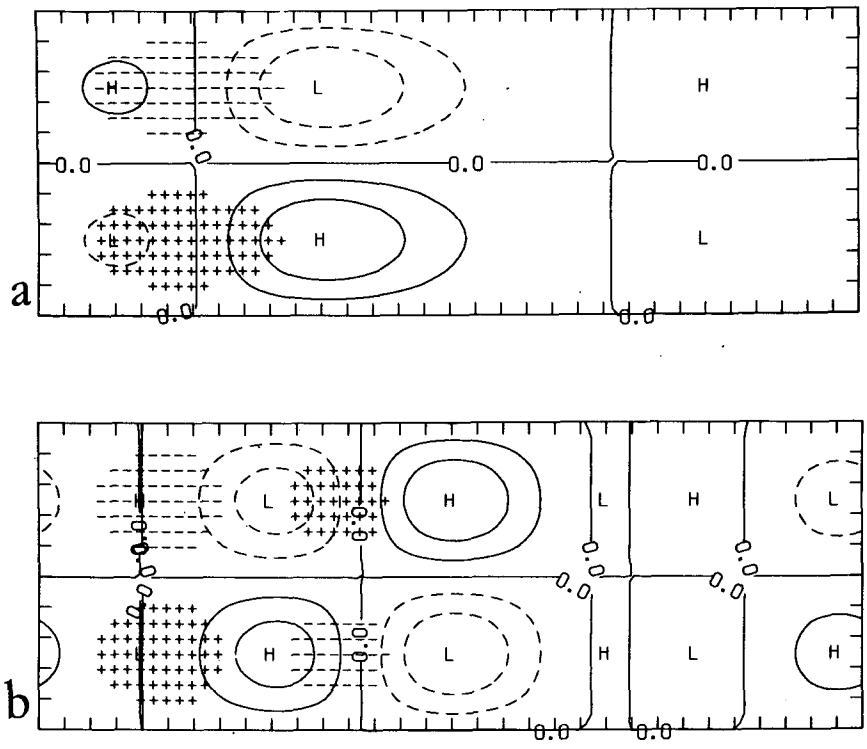

FIG. 12. As in Fig. 11, but shows only the large-scale part of the nonlinear feedback for filtered fields.

scale eigenmodes of the linearized problems. But more attractive possibilities lie in the analogy between blocking dipoles and local free modes or modons of the original quasi-geostrophic equation (McWilliams 1980). Shutts (1983) and more recently Haines and Marshall (1987) have shown how a modon can be reinforced by enslaving to its advantage incident barotropic perturbations. The limitation of this approach is that, thus far, the only known modon solution possesses a circular shape in a uniform background wind. The generation of a family of shapes with a more general background flow appears as a very difficult task for finite amplitude modes. For weakly nonlinear flows, Malguzzi and Manalotte-Rizzoli (1984) obtain a series of local and global eigenmodes by reducing the quasi-geostrophic stationary problem to a Schrödinger equation. These modes are good candidates to expand the finite amplitude quasi-stationary flows.

Our study is a self-consistent theory of the maintenance of large-scale persistent atmospheric anomalies. It confirms that a coherent structure may be obtained as the response to transient feedback. But unlike previous works, the anomaly is not directly forced, full nonlinearity is allowed and the transients are freely generated by the instability of a baroclinic jet. Owing to these factors, and in spite of its simplicity, the observed dynamics of our model compares quantitatively with the atmosphere in many respects. However, a significant discrepancy with atmospheric statistics diagnosed by Illari (1984) and Mullen (1987) is that our upper-layer feedback is almost in phase with the blocking anomaly while it seems to be located about one-quarter wavelength upstream in the atmosphere. The magnitudes of the anomalies agree very well with observations, however. Apparently, the main source of the discrepancy lies in the fact that our model is too dissipative (as a result of the lack of vertical resolution) and that the blocking anomaly largely projects on non-propagative large-scale modes. We thus believe that better agreement can be reached by allowing higher vertical resolution and a more realistic mean wind profile. Another characteristic of our model is the absence of explicit orography. This omission is acceptable in studying the variability over the Atlantic, and in western Europe but not when dealing with the Pacific case. Including orographic form drag will presumably result in triggering the phase of the blocking, although the energetics is expected to be only slightly modified. Another more serious limitation concerns the transition properties between regimes. We believe that our approach can give a good account for the maintenance of large-scale variability but the fast transitions are likely to involve mechanisms which are not represented here. For instance, the link between explosive cyclogenesis and the onset of blocking was noticed by Blackmon et al. (1986) among others. Such phenom-

ena require higher resolution, the release from quasi-geostrophic hypothesis, and the inclusion of the water cycle.

Our approach does provide, however, the basis for an operational definition of weather regimes applicable to an elaborate GCM or to atmospheric data. The difficulty is then to define the function to be minimized which must take into account the regional character of weather regimes. Beyond this step, the procedure can be applied in a straightforward way. If the number of variables describing the large-scale flow is less than, or of the order of 100, the cost of the analysis is negligible compared to the resources needed to integrate a GCM. Furthermore, the use of a 15 000-day dataset in this study is a very conservative choice. Some tests have shown that 3000 days are sufficient to characterize the weather regimes. This is not valid for the purely statistical study of persistence conducted in Part I which requires much more data. The difference lies in that a much larger amount of dynamical information is taken into account in the nonlinear equilibration. When transient fluxes data are missing, as is the case for long atmospheric records, a simplified version might be used where the tendency is fully diagnosed and estimated with finite time differences.

Persistent regimes are not the only regularities of large-scale dynamics. Extension to recurrent evolutive processes can be considered by the introduction of delays in the functional. Then propagation effects can be examined as well as the existence of systematic precursors for some flow configurations.

Acknowledgments. We thank Erland Källén, Brian Reinhold, Joe Egger, Michael Ghil and O. Talagrand for fruitful discussions and communication of some unpublished results. Brian Reinhold gave us numerous comments on the first version of this article and Claude Lemaréchal (INRIA) provided the code for quasi-Newtonian algorithm (M2QN1). The manuscript was typed by Marie-Christine Cally. The computer resources used in this study were allocated by the Scientific Council of the Centre de Calcul Vectoriel pour la Recherche. Figures were plotted by the NCAR Graphics Software.

APPENDIX A

The Quasi-Newtonian Algorithm

We recall the main features of the iterative algorithm used in order to find minima of the cost function. We use a general formulation for optimization problems and define the cost function F: $R^N \to R$ as a scalar function of the variable $x = (x_1, \cdots, x_N)^T$. Here, F is assumed to be a smooth function of x and the problem is to find the minima of F. The algorithm starts with a first guess $x^{(0)}$, and iteratively finds new approximations $x^{(n)}$ of a minumum x^* with the condition that $F(x^{(n+1)}) \leqslant F(x^{(n)})$. The general iteration formula for the quasi-Newtonian algorithm is

$$x^{(n+1)} = x^{(n)} - \lambda_n d_n, \tag{A1}$$

with

$$d_n = H_n \cdot \nabla F(x^{(n)}), \tag{A2}$$

where $\nabla F(x^{(n)})$ is the gradient of F with respect to x and H_n is a linear symmetric operator. In the Newton method, H_n is set as the inverse of the Hessian operator for $x = x^{(n)}$, namely (in orthonormal basis) the symmetric matrix containing the second-order derivatives of F. Since the computation of second-order derivatives would take a lot of computational time, the inverse Hessian operator is approximated in the quasi-Newtonian method, using the information from the gradient and previous iterations. Several algorithms may be used in this purpose; here we choose the BFGS formula:

$$H_{n+1} = H_n + \frac{\delta_n \cdot \delta_n{}^T}{\delta_n{}^T \gamma_n} - \frac{H_n \gamma_n \cdot \gamma_n{}^T H_n}{\gamma_n{}^T H_n \gamma_n} \tag{A3}$$

where

$$\delta_n = x^{(n+1)} - x^{(n)}$$

and

$$\gamma_n = \nabla F(x^{(n+1)}) - \nabla F(x^{(n)}).$$

For further details, the reader is referred to Minoux (1983). In (A1), λ_n is a scalar chosen in order to minimize

$$\phi(\lambda) = F(x^{(n)} + \lambda d_n).$$

It can be shown that the convergence of such methods is faster than exponential (superlinear), and, more precisely, that

$$\frac{\|x^{(n+1)} - x^*\|}{\|x^{(n)} - x^*\|} \to 0 \quad \text{as} \quad n \to \infty.$$

In practice, the algorithm is very efficient as soon as $x^{(n)}$ is close to the minimum (values of F about 10^{-4} times the typical initial cost) but about 100 iterations are needed to reach this stage in our problem. Improvements of this method have been developed by C. Le Maréchal (personal communication) at INRIA who gave us access to his numerical code M2QN1.

APPENDIX B

Computation of the Gradient of F

As shown in appendix A, the quasi-Newton algorithm needs to compute the gradient of the cost function F. For the sake of simplicity, we consider that the optimized variable $x = (x_1, \cdots, x_n)^T$ is built with the spectral coefficients of the two-level potential vorticity fields. Note that the associated basis is not orthonormal for the inner product defined in section 3. From (3.5) we see that the calculation of the gradient requires the knowledge of the tendency $T(L)$ and the

adjoint of the differential operator of T at LDT^*/DL defined by the formula

$$\left\langle L, \frac{DT^*}{DL}(L)\cdot L' \right\rangle = \left\langle \frac{DT}{DL}(L)\cdot L, L' \right\rangle, \quad \text{(B1)}$$

which must be valid for any vorticity fields L and L'. Since the adjunction is a linear operation, we can write separately the computation of the adjoint for the three terms A, B and C. In order to allow a compact formulation, we introduce the following operators:

$$\partial_x: \quad (q_1, q_2) \to \left(\frac{\partial q_1}{\partial x}, \frac{\partial q_2}{\partial x}\right)$$

$$\Delta: \quad (q_1, q_2) \to (\Delta q_1, \Delta q_2)$$

$$\mathrm{L}: \quad (q_1, q_2) \to (\psi_1, \psi_2)$$

$$\mathrm{L}_{\lambda_1,\lambda_2}: \quad (q_1, q_2) \to (\lambda_1 q_1, \lambda_2 q_2)$$

$$\mathrm{A}: \quad (q_1, q_2) \to \left(-U_1 \frac{\partial q_1}{\partial x}, -U_2 \frac{\partial q_2}{\partial x}\right)$$

$$\mathrm{B}: \quad (q_1, q_2) \to \left(-Q_1 \frac{\partial q_1}{\partial x}, -Q_2 \frac{\partial q_2}{\partial x}\right)$$

$$\mathrm{C}: \quad (q_1, q_2) \to (\nu_i^1 \Delta(\psi_2 - \psi_1), \nu_i^2 \Delta(\psi_1 - \psi_2))$$

$$\mathrm{D}: \quad (q_1, q_2) \to (0, -\nu_e \Delta \psi_2)$$

$$\mathrm{E}: \quad (q_1, q_2) \to \left(-\alpha \frac{\partial^8}{\partial x^8} - \beta \frac{\partial^8}{\partial y^8}\right)(q_1, q_2)$$

$$\mathrm{F}: \quad (q_1, q_2) \to (D_p(q_1), D_p(q_2))$$

where the quantities on the right-hand side of the definitions are described in section 2 of Part I.

a. Adjoint of A

Owing to our simplifications, the term A is linear and thus is identical to its differential, apart from the removal of forcing terms. Consequently, the differential of A is the sum A + B + C + D + E + F. We can compute in a formal way the adjoints of the above operators using formulas like (B1). Using the notation $\psi = (\psi_1, \psi_2)$ and $q = (q_1, q_2)$, an integration by parts shows easily that for any couple, q, q',

$$\langle q, \partial_x q' \rangle = -\langle \partial_x q, q' \rangle$$

and thus,

$$\partial_x^* = -\partial_x. \quad \text{(B2)}$$

In the same way,

$$\Delta^* = \Delta. \quad \text{(B3)}$$

Noting that the inner product (3–2) reads

$$\langle q, q' \rangle = -\iint [R_1^{-2}\psi_1 q_1' + R_2^{-2}\psi_2 q_2'] = -\iint [R_1^{-2}\psi_1' q_1 + R_2^{-2}\psi_2' q_2], \quad \text{(B4)}$$

we obtain

$$\langle q, \mathrm{L}q' \rangle = \iint [-R_1^{-2}\psi_1\psi_1' - R_2^{-2}\psi_2\psi_2']$$

and thus

$$\mathrm{L}^* = \mathrm{L}. \quad \text{(B5)}$$

Putting $\langle q, L_{\lambda_1\lambda_2} q' \rangle$ into the integral form (B4), it is seen that

$$\mathrm{L}^*_{\lambda_1,\lambda_2} = \mathrm{L}^{-1}\mathrm{L}_{\lambda_1,\lambda_2}\mathrm{L}. \quad \text{(B6)}$$

Using these elementary adjoint calculations, and the properties of adjoint composition, we compute the adjoint of the terms contained in A. Since

$$\mathrm{A} = -\mathrm{L}_{U_1,U_2}\partial_x,$$

we get

$$\mathrm{A}^* = \partial_x \mathrm{L}^{-1}\mathrm{L}_{U_1,U_2}\mathrm{L}. \quad \text{(B7)}$$

In the same way, one obtains

$$\mathrm{B}^* = \partial_x \mathrm{L}_{Q_1,Q_2}\mathrm{L}^{-1}. \quad \text{(B8)}$$

For the internal friction operator, we have

$$\langle q, \mathrm{C}q' \rangle = -\iint [\nu_i^1 R_1^{-2}\psi_1\Delta(\psi_2' - \psi_1') + \nu_i^2 R_2^{-2}\psi_2\Delta(\psi_1' - \psi_2')]$$

and since ν_i^1 is proportional to R_1^2, and ν_i^2 to R_2^2, this reads

$$\langle q_1 \mathrm{C}q' \rangle = -\lambda \iint (\psi_1 - \psi_2)\Delta(\psi_1' - \psi_2')$$

or

$$\langle q_1 \mathrm{C}q' \rangle = \lambda \iint \nabla(\psi_1 - \psi_2)\cdot\nabla(\psi_1' - \psi_2'),$$

which means that C is self-adjoint:

$$\mathrm{C}^* = \mathrm{C}. \quad \text{(B9)}$$

The Ekman damping operator is also self-adjoint, and the superviscosity as well; therefore,

$$\mathrm{D}^* = \mathrm{D} \quad \text{(B10)}$$

and

$$\mathrm{E}^* = \mathrm{E}. \quad \text{(B11)}$$

The planetary-scale damping can be decomposed as a linear combination of projections of the vorticity onto single spectral modes. Since those projections are self-adjoint and the coefficients of the combination are the same in both layers, this term is self-adjoint and again

$$\mathrm{F}^* = \mathrm{F}. \quad \text{(B12)}$$

Thus, the adjoint of A, $(DA/DL)^*$, can be simply evaluated by splitting it into elementary operators.

b. Adjoint of $\tilde{B}(L)$

First, we notice that this term is not linear in L, and thus its differentiation has to be performed before adjoint calculations. From (2.3) and (2.5), a small variation dL of the large scales induces a variation in $\tilde{B}$:

$$d\tilde{B}(L) = B(dL, \tilde{S}(L)) + B\left(L, \frac{D\tilde{S}}{DL}(L)\cdot dL\right). \tag{B13}$$

Thus, the differential of $\tilde{B}$ is the sum of two operators:

$$\text{G:}\quad (q_1, q_2) \to (J(q_1, \hat{\psi}_1) + J(\hat{q}_1, \psi_1), J(q_2, \hat{\psi}_2) + J(\hat{q}_2, \psi_2))$$

where $\hat{q}$ and $\hat{\psi}$ are fixed (actually the average small-scale part $\tilde{S}$), and H which is the composition of $B(L, \cdot)$ with the differential of $\tilde{S}$ with respect to L. Using complete notations, one obtains from (2.5):

$$\frac{D\tilde{S}}{DL}(L)\cdot dL = \sum_{i=1}^{3000} \langle \nabla_L w(L, L_i), dL\rangle \tilde{S}_i. \tag{B14}$$

The adjoint of U: $(q_1, q_2) \to (J(q_1, \hat{\psi}_1), J(q_2, \hat{\psi}_2))$ can be computed in the following way:

$$\langle q, \mathrm{U}q'\rangle = -\int\int [R_1^{-2}\psi_1 J(\hat{q}_1, \psi'_1) + R_2^{-2}\psi_2 J(\hat{q}_2, \psi'_2)]$$

or, by integration by parts,

$$\langle q, \mathrm{U}q'\rangle = +\int\int [R_1^{-2}\psi'_1 J(\hat{q}_1, \psi_1) + R_2^{-2}\psi'_2 J(\hat{q}_2, \psi_2)].$$

Here U is thus anti-adjoint:

$$\mathrm{U}^* = -\mathrm{U}. \tag{B15}$$

It can be shown in the same way that

$$\mathrm{V}^* = -\mathrm{L}^{-1}\mathrm{V}\mathrm{L}, \tag{B16}$$

where

$$\mathrm{V:}\quad (q_1, q_2) \to (J(q_1, \hat{\psi}_1), J(q_2, \hat{\psi}_2)),$$

and thus

$$\mathrm{G}^* = \mathrm{U}^* + \mathrm{V}^*$$

can be computed with the same method as A^*. Contrarily, computation of $(D\tilde{S}/DL)$ is a bit more complex. Using the L–S notations, we obtain

$$\left\langle S, \frac{D\tilde{S}}{DL}\cdot L'\right\rangle = \sum_{i=1}^{3000} \langle \nabla_L w(L, L_i), L'\rangle\langle S_i, S\rangle. \tag{B17}$$

It is noteworthy that the inner product acts here on the small-scale subspace. Since $D\tilde{S}/DL$ is a linear operator acting from the large-scale subspace to the small-scale one, its adjoint will act in the opposite way. From (B17) one may write

$$\left\langle S, \frac{D\tilde{S}}{DL}\cdot L'\right\rangle = \left\langle \sum_{i=1}^{3000} \langle S_i, S\rangle \nabla_L w(L, L_i), L'\right\rangle$$

and thus, for any small-scale field S,

$$\left(\frac{D\tilde{S}}{DL}\right)^*\cdot S = \sum_{i=1}^{3000} \langle S_i, S\rangle \nabla_L w(L, L_i).$$

This adjoint is numerically computed in this way, and composed with $B(L, \cdot)^*$ which reduces to the projection of the operator G* onto the small-scale subspace. No difficulties result from mixing adjunction and projections onto small- and large-scale subspaces since the latter are orthogonal to each other.

The gradients of the weight functions are computed using (3.8) and (3.9):

$$\nabla_L w(L, L_i) = \frac{1}{H}\left[\nabla_L \phi(d(L, L_i)) - \phi(d(L, L_i))\cdot\frac{\nabla_L H}{H}\right]$$

where

$$H = \sum_{i=1}^{3000} \phi(d(L, L_i)),$$

in such a way that we only need to know $\nabla_L \phi(d(L, L_i))$. This is evaluated by:

$$\nabla_L \phi(d(L, L_i)) = \phi'(d(L, L_i))\cdot\nabla_L d(L, L_i)). \tag{B18}$$

Numerically, the gradient of the distance in the right-hand side of (B18) is computed for the inner product associated with the Euclidian distance d. Using this norm, the gradient is written as $(L - L_i)/2d(L, L_i)$. (The singularity disappears since ϕ is actually a function of the square of the distance.) This gradient is then multiplied by a suitable constant matrix in order to get the gradient with respect to the inner product $\langle\cdot, \cdot\rangle$. Though this algebra may seem awkward, the separation into elementary operators allows straightforward numerical coding.

c. Adjoint of the term C

Using the algebra given in subsection b, the adjoint of C can be carried out in the following way. First of all, according to equation (2.6), one gets

$$\frac{D\tilde{C}}{DL}\cdot dL = \sum_{i=1}^{3000} \langle \nabla_L w(L, L_i), dL\rangle C_i,$$

and the same formulas as for $(D\tilde{S}/DL)^*$ can be derived. One then obtains

$$\left(\frac{D\tilde{C}}{DL}\right)^*\cdot L' = \sum_{i=1}^{3000} \langle C_i, L'\rangle \nabla_L w(L, L_i)$$

for any large-scale field L'. The weight gradients are estimated as previously. Once those adjoint operators are defined, $(DT/DL(L))^*$, considered as an operator, is applied to the tendency $T(L)$ and yields the gradient of the cost function.

REFERENCES

Blackmon, M. L., S. L. Mullen and G. T. Bates, 1986: The climatology of blocking events in a perpetual January simulation of a spectral general circulation model. *J. Atmos. Sci.*, **43**, 1379–1405.

Dole, R. M., and N. D. Gordon, 1983: Persistent anomalies of the extra-tropical Northern Hemisphere wintertime circulation: geographical distribution and regional persistence characteristics. *Mon. Wea. Rev.*, **111**, 1567–1586.

Fraedrich, K., and H. Bottger, 1978: A wavenumber–frequency-analysis of the 500 mb geopotential at 50°N. *J. Atmos. Sci.*, **25**, 984–1002.

Haines, P., and J. C. Marshall, 1987: Eddy-forced coherent structures as a prototype of atmospheric blocking. *Quart. J. Roy. Met. Soc.*, **113**, 681–704.

Hayashi, Y., 1982: Space–time spectral analysis and its application to atmospheric waves. *J. Meteor. Soc. Japan*, **60**, 156–171.

Illari, L., 1984: A diagnostic study of the potential vorticity in a warm blocking anticyclone. *J. Atmos. Sci.*, **41**, 3518–3526.

Itoh, H., 1985: The formation of quasi-stationary waves from the viewpoint of bifurcation theory. *J. Atmos. Sci.*, **42**, 917–932.

Legras, B., and M. Ghil, 1985: Persistent anomalies, blocking and variations in atmospheric predictability. *J. Atmos. Sci.*, **42**, 433–471.

McWilliams, J. C., 1980: An application of equivalent modons to atmospheric blocking. *Dyn. Atmos. Oceans*, **5**, 43–66.

Malguzzi, P., and P. Malanotte Rizzoli, 1984: Nonlinear stationary Rossby waves on nonuniform zonal winds and atmospheric blocking. Part I: The analytical theory. *J. Atmos. Sci.*, **41**, 2620–2628.

Minoux, M., 1983: Programmation mathématique. Théorie et algorithmes. Coll. Tech. Sci. Télécom., DUNOD, Paris, France.

Mullen, S. L., 1987: Transient eddy forcing of blocking flows. *J. Atmos. Sci.*, **44**, 3–22.

Oort, A., 1983: Global atmospheric circulation statistics, 1958–1973. NOAA Prof. Paper No. 14, U.S. Govt. Printing Office, Washington, DC, USA, 180 pp.

Pierrehumbert, R. T., 1984: Local and global baroclinic instability of a zonally varying flow. *J. Atmos. Sci.*, **41**, 2141–2162.

Reinhold, B. B., 1986: Structural determinism of linear baroclinic waves and simple non-linear equilibrium. *J. Atmos. Sci.*, **43**, 1484–1504.

——, and R. T. Pierrehumbert, 1982: Dynamics of weather regimes: Quasi-stationary waves and blocking. *Mon. Wea. Rev.*, **110**, 1105–1145.

Rex, D. F., 1950: Blocking action in the middle troposphere and its effect on regional climate. Part I: An aerological study of blocking action. *Tellus*, **2**, 196–211.

Shutts, G. J., 1983: The propagation of eddies in diffluent jetstreams: Eddy vorticity forcing of blocking flow fields. *Quart. J. R. Met. Soc.*, **109**, 737–761.

Simmons, A. J., and B. J. Hoskins, 1978: The life cycles of some nonlinear baroclinic waves. *J. Atmos. Sci.*, **35**, 414–432.

Talagrand, O., and P. Courtier, 1987: Variational assimilation of meteorological observations with the adjoint vorticity equation. Part 1: Theory. *Quart. J. Roy. Met. Soc.*, **113**, 1311–1328.

Vautard, R., 1987: Les échelles de temps de la circulation atmosphérique: Couplage interne et approches de la paramétrisation des modes rapides, thèse de Doctorat, Université Pierre et Marie Curie, Paris (in English).

——, B. Legras and M. Deque, 1988: On the source of mid-latitude low-frequency variability. Part I: A statistical approach to persistence. *J. Atmos. Sci.*, **45**, 2811–2843.

Weng, H. Y., and A. Barcilon, 1987: Favorable environments for explosive cyclogenesis in a modified two-layer eady model. *Tellus*, **39A**, 202–214.